

Nuclear matter and neutron-star properties calculated with the Skyrme interaction

J. Rikowska Stone

*Department of Physics, University of Oxford, Oxford OX1 3PU, United Kingdom
and Department of Chemistry and Biochemistry, University of Maryland, College Park, Maryland 20742, USA*

J. C. Miller

*SISSA, 34014 Trieste, Italy
and Department of Physics (Astrophysics), University of Oxford, Oxford OX1 3RH, United Kingdom*

R. Koncewicz

Department of Physics, University of Oxford, Oxford OX1 3PU, United Kingdom

P. D. Stevenson

*Department of Physics, University of Surrey, Guildford GU2 7XH, United Kingdom
and Department of Physics, University of Oxford, Oxford OX1 3PU, United Kingdom*

M. R. Strayer

Physics Division, Oak Ridge National Laboratory, Oak Ridge, Tennessee 37831-6373, USA

(Received 26 March 2003; published 23 September 2003)

The effective Skyrme interaction has been used extensively in mean-field models for several decades and many different parametrizations of the interaction have been proposed. All of these give similar agreement with the experimental observables of nuclear ground states as well as with the properties of infinite symmetric nuclear matter at the saturation density n_0 . However, when applied over a wider range of densities (up to $\sim 3n_0$) they predict widely varying behavior for the observables of both symmetric and asymmetric nuclear matter. A particularly relevant example of naturally occurring asymmetric nuclear matter is the material of which neutron stars are composed. At around nuclear matter density, this can be well represented as a mixture of neutrons, protons, electrons, and muons ($n + p + e + \mu$ matter) in β -equilibrium, and these densities turn out to be the key ones for determining the properties of neutron-star models with masses near to the widely used “canonical” value of $1.4M_\odot$. By constructing equations of state for neutron-star matter using the different Skyrme parametrizations, calculating corresponding neutron-star models and then comparing these with observational data, an additional constraint can be obtained for the values of the Skyrme parameters. Such a constraint is particularly relevant because the parametrizations are initially determined by fitting to the properties of doubly closed-shell nuclei and it is an open question how suitable they then are for nuclei with high values of isospin, such as those at the neutron drip-line and beyond. The neutron-star environment provides an invaluable testing ground for this. We have carried out an investigation of 87 different Skyrme parametrizations in order to examine how successful they are in predicting the expected properties of infinite nuclear matter and generating plausible neutron-star models. This is the first systematic study of the predictions of the various Skyrme parametrizations for the density dependence of the characteristic observables of nuclear matter; the density dependence of the symmetry energy for β -equilibrium matter turns out to be a crucial property for indicating which Skyrme parameter sets will apply equally well for finite nuclei and for neutron-star matter. Only 27 of the 87 parametrizations investigated pass the test of giving satisfactory neutron-star models and we present a list of these.

DOI: 10.1103/PhysRevC.68.034324

PACS number(s): 21.60.Jz, 26.60.+c, 21.30.Fe

I. INTRODUCTION

In order to calculate neutron-star models, it is necessary to have an equation of state linking pressure and total energy density and, for obtaining this, expressions must be supplied for the interaction potentials of the particles concerned. In the case of the nucleon-nucleon potential, various approaches have been followed, both relativistic and nonrelativistic [1–3] reflecting the situation in low-energy nuclear structure physics where both relativistic and nonrelativistic models are used without there being any clear preference for one or the other. It is necessary to make assumptions about

the nature of the hadron-hadron potentials which are not well known, particularly as regards their behavior as a function of density.

The nucleon-nucleon potentials fall into two classes described as “realistic” and “phenomenological.” The “realistic” ones are model based but are constructed so as to fit experimental data for free nucleon-nucleon scattering and properties of the deuteron. This is done by obtaining a best fit for a large number of adjustable parameters (typically 40–60) using several thousand experimental data points [4–6]. The quality of these potentials then clearly depends on that of the experimental data used. All of them involve a long-

range one-pion exchange part and they differ mainly in their treatment of the intermediate and short-range terms. The most recently developed and frequently used ones include the Reid-93, Nijmegen II [4] and Argonne v_{18} (A18) [5] potentials (all local and nonrelativistic), the Nijmegen II potential [4] (nonlocal and nonrelativistic), and the CD-Bonn potential [6] (nonlocal and relativistic). For use in describing dense nuclear matter, they need to be renormalized and this involves using many-body techniques. The Brueckner-Hartree-Fock method, based on selective summation of diagrams in perturbation theory, is applicable to both nonrelativistic (Brueckner-Hartree-Fock) potentials [7–9] and relativistic (Dirac-Brueckner) ones [10]. Since this selective summation is rather hard to do in practice, an alternative variational method [11,12] has been developed for nonrelativistic potentials (with and without relativistic boost corrections) [13,14], providing a systematic approximation to diagrams which cannot be calculated exactly. In all of these methods, the energy per particle \mathcal{E} is calculated for symmetric nuclear matter (SNM) and pure neutron matter (PNM). However, this is not directly applicable for neutron-star matter, which comes between these two extreme cases and also includes other types of particle. Some kind of “interpolation” needs to be made between the SNM and PNM cases [9]. In their work calculating an equation of state (EOS) for multicomponent dense matter, Akmal *et al.* [14] fitted a smooth function to the calculated density dependence of the energy per particle in SNM and PNM so that derivatives could be obtained and the chemical potentials and other properties could be calculated [15]. The equilibrium composition of the matter was then obtained by interpolation between the SNM and PNM results. The phenomenological Skyrme-like interactions FPS [14,16] and FPS21 [17] (with ~ 20 fitting parameters) were used for this purpose, although the simpler SKM [18,19] and Skyrme1' [16,17] Skyrme interactions (with ~ 10 adjustable parameters) were also used.

The so-called phenomenological models are much simpler. Both relativistic and nonrelativistic approaches are used in the literature. The relativistic ones use relativistic mean field (RMF) theory with the effective interaction being represented by a Lagrangian, dependent on a number of coupling constants, which is fitted to the saturation properties of nuclear matter and the observables of the ground states of finite nuclei [20]. The equations of motion for baryons and mesons are solved self-consistently using the Hartree technique. The RMF approach is appealing because it naturally contains the appropriate degrees of freedom for high density matter, including baryons interacting through the exchange of scalar and vector mesons. However, as has been discussed recently [14], there are some doubts about the validity of the mean-field approximation for the meson fields used in RMF theory in the density region $(1-5)n_0$ (nuclear saturation density) which is relevant for neutron stars.

The nonrelativistic models use the Hartree-Fock or Extended-Thomas-Fermi-Strutinsky-Integral [21] techniques to solve for the nucleonic equations of motion based on a Hamiltonian utilizing an effective nucleon-nucleon interaction of the Skyrme [22,23], Gogny [24–26], or separable monopole (SMO) [27,28] types. These models can be sur-

prisingly successful for describing dense matter at up to $(2-3)n_0$, depending on the choice of the effective interaction. In this density region, we consider only β -equilibrium matter (BEM) consisting of neutrons, protons, electrons, and muons ($n+p+e+\mu$) and neglect the possible presence of mesons, and strange baryons. Nevertheless, EOS's constructed under these restrictions work very well, even when extrapolated to higher densities, and give a reasonable description of neutron stars.

In a previous paper [28] we examined the performance of the effective separable monopole interaction when used for symmetric and asymmetric nuclear matter and for constructing an EOS for neutron-star matter using a mean-field Hartree-Fock approximation. Comparing results obtained with the SMO and with a selected set of Skyrme interactions led to the intriguing conclusion that some predictions for the properties of nuclear matter are very sensitive to the particular choice of parametrization for the Skyrme potential. This provided the motivation for the present study.

The Skyrme nucleon-nucleon interaction has been used in nuclear Hartree-Fock calculations since the 1970s. There are many known parametrizations of it which reproduce experimental data for the ground states of finite nuclei and for the observables of infinite nuclear matter at the saturation density, giving more or less comparable agreement with experimental or expected empirical data. It has long been recognized that infinite nuclear matter is not only an idealized system for testing nucleon-nucleon potentials but is also a good approximation for the matter occurring in some actual physical objects: neutron stars. In turn, the neutron star environment has direct relevance for the structure of unstable nuclei. In particular, there is increasing interest in the nuclear symmetry energy because it has been shown that this significantly affects the binding energies and radii of neutron-rich nuclei in RMF models [29]. Accurate knowledge is needed of the density dependence of the symmetry energy in order to understand the behavior of the matter radii of neutron-rich isotopes, which increase with A faster than the usually expected $A^{1/3}$ relation, and to explain the experimental indication that the density at the center of neutron-rich nuclei is lower than that for nuclei close to the β -stability line [30,31]. A connection between neutron radii in nuclei and in pure neutron matter has recently been investigated [32]. The equation of state of high density nuclear matter is also important for studies of heavy-ion collisions at intermediate and high energies. Bao-An Li *et al.* [33] have studied the ratio of protons and neutrons in the pre-equilibrium state of nuclear matter after neutron-rich heavy-ion collisions as a function of kinetic energy and the incompressibility modulus. Very recently, Bao-An Li [34] has proposed a novel way to constrain predictions for the behavior of the nuclear symmetry energy at high densities using an isospin-dependent hadronic transport model. The experimental probes considered are the π^- to π^+ ratio and the neutron-proton collective flow. As we will see later, the nuclear symmetry energy and, consequently, the proton/neutron ratio are crucial factors in constructing an EOS for asymmetric nuclear matter based on nucleon-nucleon interactions.

In this paper we investigate the properties of infinite sym-

metric and asymmetric nuclear matter, calculated as functions of density, for a wide range of Skyrme models. By construction, all of these models already give plausible results for finite nuclei. After describing the calculation procedure in Sec. II, we summarize the results for infinite symmetric and asymmetric nuclear matter in Sec. III, selecting as suitable Skyrme parametrizations the ones which satisfy the expected constraints for nuclear matter properties. For each acceptable set of Skyrme parameters we then construct an EOS for neutron-star matter and calculate the predicted properties of corresponding neutron-star models. In Sec. IV, we draw conclusions concerning the Skyrme parameter sets which seem to remain viable on the basis of these considerations.

II. THE CALCULATION PROCEDURE

A. The Skyrme interaction

The general form of the effective Skyrme interaction, as used for describing finite nuclei in mean-field models, is well known (see, for example, the references given below in this section). The total binding energy of a nucleus can be expressed as the integral of a density functional \mathcal{H} which is given as a function of empirical parameters [23],

$$\mathcal{H} = \mathcal{K} + \mathcal{H}_0 + \mathcal{H}_3 + \mathcal{H}_{eff} + \dots, \quad (1)$$

where \mathcal{K} is the kinetic-energy term and the \mathcal{H}_0 (zero-range), \mathcal{H}_3 (density-dependent), and \mathcal{H}_{eff} (effective-mass-dependent) terms, which are relevant for calculating the properties of nuclear matter, are functions of nine parameters t_0 , t_1 , t_2 , t_3 , x_0 , x_1 , x_2 , x_3 , and α , and are given as follows:

$$\mathcal{H}_0 = \frac{1}{4}t_0[(2+x_0)n^2 - (2x_0+1)(n_p^2 + n_n^2)], \quad (2)$$

$$\mathcal{H}_3 = \frac{1}{24}t_3n^\alpha[(2+x_3)n^2 - (2x_3+1)(n_p^2 + n_n^2)], \quad (3)$$

$$\begin{aligned} \mathcal{H}_{eff} = & \frac{1}{8}[t_1(2+x_1) + t_2(2+x_2)]\tau n \\ & + \frac{1}{8}[t_2(2x_2+1) - t_1(2x_1+1)](\tau_p n_p + \tau_n n_n). \end{aligned} \quad (4)$$

The kinetic-energy term is added in a form used in the Fermi gas model for noninteracting fermions, $\mathcal{K} = (\hbar^2/2m)\tau$. In Eqs. (2)–(4), the total nuclear number densities n and kinetic-energy densities τ are defined as $n = n_n + n_p$ and $\tau = \tau_n + \tau_p$.

Eighty-seven parametrizations of the Skyrme interaction, published since 1972 [35], were selected for the analysis presented in this paper. In the order of publication date, these are as follows: SI and SII [22], SkT [36], SIII, SIV, SV, SVI [37], SVII, SIII* [38], SkM [18], SGI, SGII [39], SkM* [40], RATP [41], SkT1-SkT9 [42], SkP [43], E, Es, Z, Zs, Zs*, Rs, Gs [44], SkMP [45], SkSC1-SkSC3 [46], SkSC4 [47], SkSC5, SkSC6, SkSC10 [21], SkI1-SkI5 [48], SLy1-SLy10 [49], SkM1 [50], Skyrme1' [17], SkI6 [51], SLy230a [23], SKXce, SKXm, SKX [52], SkO, SkO' [53], MSk1-MSk6 [54], SKRA [55], MSk7 [56], MSk5*, v110-v070 [57], BSk1 [58] and Skz-1, Skz0-4 [59]. The list is not fully

comprehensive but it gives a representative sample of the Skyrme interactions used in nuclear physics applications.

We note that in some cases these parametrizations are members of “families” developed by single research groups (e.g., the SLy or SkI interactions) which differ only in the treatment of the center-of-mass motion, the spin-orbit interaction, or the set of experimental data to which they are fitted. However, in order to accommodate the changes and still keep a good agreement with the data for finite nuclei, the full set of parameters needs to be refitted, including those which are most relevant for infinite nuclear matter. As there are strong correlations among the parameters of each set, it cannot be guaranteed that even small changes in the individual parameters will not together produce a significantly different correlated effect. We therefore examine all members of parametrization families as independent sets.

B. Infinite symmetric and asymmetric nuclear matter

A detailed account of the quantities describing nuclear matter properties and their expected values can be found in recent publications [23,28] where their explicit form in terms of the Skyrme interaction parameters is also given. These quantities can be expressed generally as functions of the total nucleon number density n in fm^{-3} (the symbol ρ is used throughout this work for the mass density in g/cm^3) and the asymmetry parameter

$$I = \frac{N-Z}{A}, \quad (5)$$

where N is the number of neutrons, Z is the number of protons, and A is the total baryon number. The proton and neutron number densities are then given in terms of I and n by

$$n_p = \frac{1}{2}(1-I)n, \quad (6)$$

$$n_n = \frac{1}{2}(1+I)n. \quad (7)$$

The total binding energy per particle, denoted by $\mathcal{E}(n, I)$, is used for calculating the *pressure* P in nuclear matter [1]:

$$P(n, I) = n^2 \frac{\partial \mathcal{E}}{\partial n} = n \frac{\partial \epsilon}{\partial n} - \epsilon, \quad (8)$$

where $\epsilon = n(\mathcal{E} + mc^2)$ is the total energy density and m is the nucleon mass. The *incompressibility modulus* K of SNM is given by [23]

$$K(n, I) = 9n^2 \frac{\partial^2 \mathcal{E}}{\partial n^2} + 18 \frac{P(n, I)}{n}. \quad (9)$$

The speed of sound v_s is related to K by

$$\frac{v_s}{c} = \sqrt{\frac{K}{9(mc^2 + \mathcal{E} + P/n)}}. \quad (10)$$

Another important variable for discussions of asymmetric nuclear matter is the *symmetry energy* \mathcal{S} , defined as the difference in energy between symmetric and pure neutron matter

$$\mathcal{S}(n) = \mathcal{E}(n, I=0) - \mathcal{E}(n, I=1). \quad (11)$$

$\mathcal{S}(n)$ can be expanded about the value of the energy for symmetric nuclear matter [1] with the second-order term being related to the *asymmetry coefficient* a_s in the semiempirical mass formula

$$a_s = \frac{1}{2} \left. \frac{\partial^2 \mathcal{E}}{\partial I^2} \right|_{I=0}. \quad (12)$$

Finally, the *isoscalar* and *isovector* effective nucleon masses in infinite nuclear matter (denoted by m_s^*/m and m_v^*/m , respectively, measured in units of the vacuum nucleon mass m) can be written as functions of the Skyrme parameters and the density of the medium [23]. The effective neutron mass in dense asymmetric matter is then given by [60]

$$\frac{\hbar^2}{m_n^*} = (1+I) \frac{\hbar^2}{m_s^*} - I \frac{\hbar^2}{m_v^*}; \quad (13)$$

for protons the sign of I in the above equation is reversed.

The specific case of SNM is described by the *equilibrium density* n_0 and three quantities calculated at this density: the *binding energy per particle* $\mathcal{E}_0 = \mathcal{E}(n_0, I=0)$, the *incompressibility modulus* K_∞ , and the *isoscalar effective mass* (m_s^*/m).

The two extreme states of infinite nuclear matter, SMN ($I=0$) and PNM ($I=1$), have fundamentally different properties. The energy per particle \mathcal{E} in SNM reaches a negative minimum value (i.e., it saturates) at a *saturation density* n_0 , and this then corresponds to a bound state of SNM. The value of \mathcal{E} at saturation is usually taken to be the coefficient of the volume term a_v in the liquid-drop model, obtained by fitting with the binding energies of a large number of nuclei. This procedure gives $\mathcal{E}_0 = -(16.0 \pm 0.2)$ MeV [23]. However, a somewhat lower value [$\mathcal{E}_0 = -(15.6 \pm 0.2)$ MeV] has been quoted recently by Heiselberg and Hjorth-Jensen [1]. The density n_0 of SNM at saturation is expected to be $n_0 = 0.16 \pm 0.005 \text{ fm}^{-3}$ [23] based on calculating the charge distribution in heavy nuclei. \mathcal{E} in PNM is predicted to be always positive, i.e., PNM does not exist in a bound state. This property of PNM places a powerful constraint on the parameters of the Skyrme interaction, as will be discussed later.

C. β -equilibrium $n+p+e+\mu$ matter

More insight into the validity of the various Skyrme parametrizations can be obtained by investigating the density dependence of the properties of nuclear matter in the region beyond nuclear saturation density (at $n_0 \sim 0.16 \text{ fm}^{-3}$). As the density is increased from n_0 up to $(2-3)n_0$, the nuclear matter (which at low densities consists of nucleons bound in atomic nuclei at saturation) becomes first a system of un-

bound neutrons, protons, and electrons existing in equilibrium with respect to weak interactions (making the usual assumption that neutrinos leave the system and thus are not contributing to the equilibrium conditions) but then, as a threshold density is passed, becomes a mixture of neutrons, protons, electrons, and muons. This form of matter is characterized by the following processes:

$$n \leftrightarrow p + e^- \leftrightarrow p + \mu^-.$$

Equilibrium implies that the chemical potentials should satisfy the following conditions (from now on, we use e and μ in place of e^- and μ^-):

$$\mu_n = \mu_p + \mu_e, \quad \mu_\mu = \mu_e, \quad (14)$$

with each μ being defined by

$$\mu_j = \frac{\partial \epsilon}{\partial n_j}, \quad (15)$$

where ϵ is the total energy density (including the rest masses of the particles involved) and the n_j 's are the particle number densities. The latter are used to define particle fractions with respect to the total baryon number density $n_b = n_n + n_p$:

$$y_j = \frac{n_j}{n_b}. \quad (16)$$

The requirement of charge neutrality of the matter implies $n_p = n_e + n_\mu$.

We need to study the composition of this phase of matter and, in particular, the values taken by the proton fraction y_p which has relevance for the cooling mechanism of neutron-stars, as discussed in Ref. [28]. The proton fraction is related to the asymmetry parameter I , introduced earlier, by $I = 1 - 2y_p$ and can also be expressed in terms of the symmetry energy [Eq. (11)] by [1]

$$\hbar c (3\pi^2 n y_p)^{1/3} = 4\mathcal{S}(n)(1 - 2y_p). \quad (17)$$

An equation of state for zero-temperature β -stable nucleon+lepton matter can be constructed from the Skyrme interaction following the procedure described previously (see, e.g., Refs. [23,28]). The total energy density of the $n+p+e+\mu$ matter is written as the sum of the nucleon and lepton contributions [23]:

$$\begin{aligned} \epsilon(n_p, n_n, n_e, n_\mu) = & \epsilon_N(n_p, n_n) + n_n m_n c^2 + n_p m_p c^2 + \epsilon_e(n_e) \\ & + \epsilon_\mu(n_\mu), \end{aligned} \quad (18)$$

where $\epsilon_N = n_b \mathcal{E}_N$. Given these definitions and conditions, the EOS is determined by two expressions:

$$\rho(n_b) = \frac{\epsilon(n_b)}{c^2}, \quad P(n_b) = n_b^2 \frac{d(\epsilon/n_b)}{dn_b}, \quad (19)$$

where ρ is the mass density of the matter. The form used here for the EOS is obtained by eliminating n_b between Eqs. (19) and giving the pressure as a function of the mass density ρ .

D. Neutron stars

A neutron star is composed of matter at densities ranging from that of terrestrial iron up to several times that of nuclear matter and, for describing this theoretically, it is necessary to use a variety of models of atomic and nuclear interactions. From the lowest densities up to $\rho \sim 4.3 \times 10^{11} \text{ g/cm}^3$ (the neutron-drip point [61]), the matter is in the form of a nuclear lattice with the nuclei going from those of the iron group up to progressively more neutron-rich ones as the density increases. The electrons are initially clustered around the nuclei but form an increasingly uniform free electron gas with rising density. Beyond the neutron-drip point, free neutrons appear. Above $\sim 2 \times 10^{14} \text{ g/cm}^3$, nuclei no longer exist and the matter consists of nucleon and electron fluids; with further increases of density, muons appear in coexistence with the neutrons, protons, and electrons in β -equilibrium. At even higher densities, heavier mesons and strange baryons are believed to play a role (see, e.g., Ref. [62] and references therein, [63–66]). Ultimately, at the center of the star, a quark matter phase may appear, either alone or coexisting with hadronic matter [20,67].

In the present work, we will only be modeling the nucleon + lepton phase of neutron-star matter. Since only part of the star is in this phase, the calculated EOS needs to be matched, at lower and (possibly) higher densities, onto other equations of state reflecting the composition of matter at those densities. For lower densities, we have used the Baym-Pethick-Sutherland (BPS) EOS [61], matching onto the Skyrme EOS at $n \sim 0.1 \text{ fm}^{-3}$ and going down to $n \sim 6.0 \times 10^{-12} \text{ fm}^{-3}$. Although it has been argued that extrapolation of our type of EOS to higher densities is not unreasonable [14,23] and that the error made by not including the heavy baryons and possible quarks in the calculation may not be significant, we prefer to limit our discussion to the density region where our models for the $n + p + e + \mu$ gas are believed to be strictly valid. For example, we do not regard these models as being suitable for calculating reliably the maximum mass of a neutron star, since this is determined mainly by the high density part of the EOS, which should be properly matched onto that for the nucleon + lepton gas considered here. However, they are mainly satisfactory for considering stars at around the “canonical” mass of $1.4M_\odot$.

Using a tabulated form of the composite EOS’s, we numerically integrated the Tolman-Oppenheimer-Volkov equation [28,68]

$$\frac{dP}{dr} = - \frac{Gm(r)\rho (1 + P/\rho c^2)(1 + 4\pi r^3 P/m(r)c^2)}{r^2 (1 - 2Gm(r)/rc^2)} \quad (20)$$

with

$$m(r) = \int_0^r 4\pi r'^2 \rho(r') dr' \quad (21)$$

to obtain sequences of neutron-star models with a range of values for the central density. Integration of Eqs. (20) and (21), for any specified central density, gives directly the corresponding values for the total gravitational mass M and radius R of the star (the surface being at the location where the pressure vanishes). Only models with radii larger than that of the maximum-mass model are stable to radial oscillations (a requirement in order for the model to represent a realistic neutron star).

We have also calculated some other key properties of our neutron-star models. The total baryon number A is given by

$$A = \int_0^R \frac{4\pi r^2 n_b(r) dr}{(1 - 2Gm(r)/rc^2)^{1/2}} \quad (22)$$

and the binding energy released in a supernova core collapse, forming the neutron-star, is approximately $E_{bind} = (Am_0 - M)c^2$, where m_0 is the mass per baryon of ^{56}Fe . Analysis of data from supernova 1987A leads to an estimate of $E_{bind} = (3.8 \pm 1.2) \times 10^{53} \text{ ergs}$ [69].

Another quantity of interest for possible comparison with observational data is the minimum rotation period τ_{min} (see Ref. [20]). The minimum period is given by the centrifugal balance condition for an equatorial fluid element (i.e., the condition for it to be moving on a circular geodesic). While determining this accurately requires using a numerical code for constructing general-relativistic models of rapidly rotating stars, quite good values can be obtained from results for nonrotating models using the empirical formula [70,71]

$$\tau_{min} = 0.82 \left(\frac{M_{max}}{M_\odot} \right)^{-1/2} \left(\frac{R_{max}}{10 \text{ km}} \right)^{3/2} \text{ ms}, \quad (23)$$

where M_{max} and R_{max} are the gravitational mass and radius of the *maximum-mass* nonrotating model for the given EOS. The shortest period so far observed is 1.56 ms [20] but it is possible that this limit may be connected with the techniques used for measuring pulsar periods rather than being a genuine physical limit.

III. RESULTS AND DISCUSSION

In this section we discuss predictions for the physical quantities, defined in the preceding section, as given by different parameter sets of the Skyrme interaction. Since there is a limited amount of decisive experimental and observational evidence which can be used for comparing with these, we are often left with a rather wide range of acceptable values or have to compare our results with the ones obtained with other theoretical models. The region of particle number densities considered here, as mentioned in the preceding section, is $0.1 \leq n \leq 0.5 \text{ fm}^{-3}$ which goes up to approximately three times the nuclear saturation density. It is assumed that the Skyrme model is valid within this range for the evaluation of the nucleon energy density and related quantities.

Giving satisfactory values for the standard properties of SNM at nuclear saturation density (see Table I) is a usual requirement imposed for determining the parameters of the Skyrme interaction. Most of the potentials considered here

TABLE I. Properties of symmetric nuclear matter at nuclear saturation density n_0 (fm^{-3}) as predicted by different types of Skyrme interaction: Fermi momentum k_F (fm^{-1}), mean distance between adjacent nucleons $r_0 = (9\pi)^{1/3}/2k_F$ (fm), total binding energy per particle \mathcal{E} (MeV), incompressibility modulus K_∞ (MeV), asymmetry coefficient a_s (MeV), speed of sound v_s/c , and the isoscalar effective mass $m_{eff} = m_s^*/m$.

| Skyrme | n_0 | k_F | r_0 | \mathcal{E} | a_s | K_∞ | v_s | m_{eff} | Skyrme | n_0 | k_F | r_0 | \mathcal{E} | a_s | K_∞ | v_s | m_{eff} |
|--------|-------|-------|-------|---------------|-------|------------|-------|-----------|---------|-------|-------|-------|---------------|-------|------------|-------|-----------|
| SI | 0.156 | 1.320 | 1.154 | -15.99 | 29.25 | 372.1 | 0.212 | 0.91 | SLy0 | 0.160 | 1.334 | 1.142 | -15.97 | 32.03 | 230.7 | 0.167 | 0.70 |
| SII | 0.148 | 1.300 | 1.172 | -15.96 | 34.15 | 341.6 | 0.203 | 0.58 | SLy1 | 0.161 | 1.334 | 1.141 | -15.98 | 32.04 | 230.8 | 0.167 | 0.70 |
| SKT | 0.148 | 1.298 | 1.174 | -15.40 | 24.90 | 334.0 | 0.200 | 0.60 | SLy2 | 0.161 | 1.335 | 1.141 | -15.99 | 32.05 | 230.9 | 0.167 | 0.70 |
| SIII | 0.145 | 1.291 | 1.180 | -15.85 | 28.17 | 355.9 | 0.207 | 0.76 | SLy3 | 0.161 | 1.335 | 1.141 | -15.97 | 32.03 | 230.9 | 0.167 | 0.70 |
| SIV | 0.151 | 1.308 | 1.165 | -15.96 | 31.24 | 325.4 | 0.198 | 0.47 | SLy4 | 0.160 | 1.332 | 1.143 | -15.97 | 32.04 | 230.9 | 0.167 | 0.69 |
| SV | 0.155 | 1.320 | 1.154 | -16.05 | 32.86 | 306.8 | 0.192 | 0.38 | SLy5 | 0.161 | 1.335 | 1.141 | -15.98 | 32.05 | 230.9 | 0.167 | 0.70 |
| SVI | 0.144 | 1.286 | 1.185 | -15.75 | 26.89 | 364.0 | 0.209 | 0.95 | SLy6 | 0.159 | 1.331 | 1.145 | -15.92 | 32.00 | 230.8 | 0.167 | 0.69 |
| SVII | 0.143 | 1.285 | 1.185 | -15.79 | 26.96 | 366.9 | 0.210 | 1.00 | SLy7 | 0.159 | 1.329 | 1.146 | -15.90 | 32.03 | 230.6 | 0.167 | 0.69 |
| SIII* | 0.151 | 1.307 | 1.165 | -16.57 | 32.67 | 372.9 | 0.212 | 0.79 | SLy8 | 0.161 | 1.334 | 1.141 | -15.97 | 32.04 | 230.9 | 0.167 | 0.70 |
| SkM | 0.160 | 1.334 | 1.142 | -15.77 | 30.77 | 217.5 | 0.162 | 0.79 | SLy9 | 0.151 | 1.308 | 1.164 | -15.79 | 32.02 | 230.3 | 0.166 | 0.67 |
| SGI | 0.155 | 1.318 | 1.156 | -15.89 | 28.35 | 262.6 | 0.178 | 0.61 | SLy10 | 0.156 | 1.321 | 1.153 | -15.90 | 32.02 | 230.4 | 0.167 | 0.68 |
| SGII | 0.159 | 1.329 | 1.146 | -15.59 | 26.85 | 215.4 | 0.161 | 0.79 | SkM1 | 0.160 | 1.334 | 1.142 | -15.77 | 25.19 | 217.5 | 0.162 | 0.79 |
| SkM* | 0.160 | 1.334 | 1.142 | -15.77 | 30.06 | 217.5 | 0.162 | 0.79 | Skymel' | 0.156 | 1.320 | 1.154 | -15.99 | 29.37 | 372.1 | 0.211 | 0.91 |
| RATP | 0.160 | 1.333 | 1.143 | -16.05 | 29.28 | 240.6 | 0.170 | 0.67 | SkI6 | 0.159 | 1.331 | 1.144 | -15.92 | 30.13 | 249.7 | 0.173 | 0.64 |
| SkT1 | 0.161 | 1.336 | 1.140 | -15.98 | 32.05 | 237.2 | 0.169 | 1.00 | SkXce | 0.155 | 1.320 | 1.154 | -15.86 | 30.16 | 269.1 | 0.180 | 1.01 |
| SkT2 | 0.161 | 1.336 | 1.140 | -15.94 | 32.03 | 236.8 | 0.169 | 1.00 | SkXm | 0.159 | 1.330 | 1.145 | -16.04 | 31.22 | 239.1 | 0.170 | 0.97 |
| SkT3 | 0.161 | 1.336 | 1.140 | -15.94 | 31.53 | 236.8 | 0.169 | 1.00 | SkX | 0.156 | 1.321 | 1.153 | -16.05 | 31.11 | 272.0 | 0.181 | 0.99 |
| SkT4 | 0.159 | 1.331 | 1.145 | -15.95 | 35.49 | 236.5 | 0.169 | 1.00 | MSk1 | 0.158 | 1.326 | 1.148 | -15.83 | 30.02 | 234.6 | 0.168 | 1.00 |
| SkT5 | 0.164 | 1.345 | 1.133 | -16.00 | 37.05 | 202.7 | 0.156 | 1.00 | MSk2 | 0.158 | 1.326 | 1.148 | -15.83 | 30.02 | 232.5 | 0.167 | 1.05 |
| SkT6 | 0.161 | 1.336 | 1.140 | -15.96 | 29.99 | 237.0 | 0.169 | 1.00 | MSk3 | 0.158 | 1.327 | 1.148 | -15.82 | 28.00 | 234.4 | 0.168 | 1.00 |
| SkT7 | 0.161 | 1.335 | 1.141 | -15.94 | 29.54 | 236.7 | 0.169 | 0.83 | MSk4 | 0.158 | 1.326 | 1.148 | -15.79 | 28.01 | 232.0 | 0.167 | 1.05 |
| SkT8 | 0.161 | 1.335 | 1.141 | -15.94 | 29.95 | 236.8 | 0.169 | 0.83 | MSk5 | 0.158 | 1.326 | 1.148 | -15.79 | 28.01 | 232.0 | 0.167 | 1.05 |
| SkT9 | 0.161 | 1.334 | 1.142 | -15.88 | 29.78 | 235.9 | 0.169 | 0.83 | MSk5* | 0.156 | 1.322 | 1.152 | -15.78 | 28.01 | 244.6 | 0.172 | 0.80 |
| SkP | 0.163 | 1.341 | 1.136 | -15.95 | 30.02 | 201.9 | 0.156 | 1.00 | MSk6 | 0.158 | 1.326 | 1.148 | -15.79 | 28.01 | 232.0 | 0.167 | 1.05 |
| E | 0.159 | 1.331 | 1.144 | -16.12 | 27.65 | 335.3 | 0.201 | 0.87 | MSk7 | 0.158 | 1.326 | 1.148 | -15.79 | 27.96 | 232.1 | 0.167 | 1.05 |
| Es | 0.163 | 1.341 | 1.136 | -16.02 | 26.44 | 249.9 | 0.173 | 0.84 | SKRA | 0.160 | 1.332 | 1.144 | -15.78 | 31.35 | 217.9 | 0.162 | 0.75 |
| Z | 0.159 | 1.331 | 1.145 | -15.97 | 26.81 | 332.1 | 0.200 | 0.84 | SkO | 0.161 | 1.335 | 1.141 | -15.83 | 32.01 | 224.3 | 0.164 | 0.90 |
| Zs | 0.163 | 1.342 | 1.135 | -15.88 | 26.70 | 234.5 | 0.168 | 0.78 | SkO' | 0.160 | 1.334 | 1.142 | -15.75 | 31.98 | 223.3 | 0.164 | 0.90 |
| Zs* | 0.163 | 1.340 | 1.136 | -15.96 | 28.82 | 236.0 | 0.169 | 0.77 | SLy230a | 0.160 | 1.333 | 1.142 | -15.99 | 32.04 | 230.9 | 0.167 | 0.70 |
| Rs | 0.158 | 1.327 | 1.148 | -15.59 | 30.61 | 238.3 | 0.169 | 0.78 | v110 | 0.158 | 1.326 | 1.148 | -15.79 | 28.01 | 232.0 | 0.167 | 1.05 |
| Gs | 0.158 | 1.327 | 1.148 | -15.59 | 31.40 | 238.1 | 0.169 | 0.78 | v105 | 0.158 | 1.326 | 1.148 | -15.79 | 28.01 | 232.0 | 0.167 | 1.05 |
| SkMP | 0.157 | 1.325 | 1.149 | -15.56 | 29.91 | 231.7 | 0.167 | 0.65 | v100 | 0.158 | 1.326 | 1.148 | -15.79 | 28.01 | 232.0 | 0.167 | 1.05 |
| SkSC1 | 0.161 | 1.335 | 1.141 | -15.85 | 28.11 | 235.6 | 0.168 | 1.00 | v090 | 0.158 | 1.326 | 1.148 | -15.79 | 28.01 | 232.0 | 0.167 | 1.05 |
| SkSC2 | 0.161 | 1.335 | 1.141 | -15.90 | 24.75 | 236.2 | 0.169 | 1.00 | v080 | 0.158 | 1.326 | 1.148 | -15.79 | 28.01 | 232.0 | 0.167 | 1.05 |
| SkSC3 | 0.161 | 1.335 | 1.141 | -15.85 | 27.02 | 235.5 | 0.168 | 1.00 | v075 | 0.158 | 1.326 | 1.148 | -15.80 | 28.01 | 232.1 | 0.167 | 1.05 |
| SkSC4 | 0.161 | 1.335 | 1.141 | -15.86 | 28.82 | 235.8 | 0.168 | 1.00 | v070 | 0.158 | 1.326 | 1.148 | -15.80 | 28.00 | 232.1 | 0.167 | 1.05 |
| SkSC5 | 0.161 | 1.335 | 1.141 | -15.85 | 31.00 | 235.6 | 0.168 | 1.00 | BSk1 | 0.157 | 1.326 | 1.149 | -15.80 | 27.82 | 232.1 | 0.167 | 1.05 |
| SkSC6 | 0.161 | 1.336 | 1.141 | -15.92 | 24.59 | 236.5 | 0.169 | 1.00 | Skz-1 | 0.160 | 1.334 | 1.142 | -16.00 | 32.02 | 231.1 | 0.167 | 0.70 |
| SkSC10 | 0.161 | 1.336 | 1.141 | -15.96 | 22.84 | 237.0 | 0.169 | 1.00 | Skz0 | 0.160 | 1.334 | 1.142 | -16.00 | 32.02 | 231.1 | 0.167 | 0.70 |
| SkI1 | 0.161 | 1.335 | 1.141 | -15.95 | 37.59 | 243.8 | 0.171 | 0.69 | Skz1 | 0.160 | 1.334 | 1.142 | -16.00 | 32.03 | 231.1 | 0.167 | 0.70 |
| SkI2 | 0.158 | 1.327 | 1.148 | -15.77 | 33.42 | 241.9 | 0.171 | 0.68 | Skz2 | 0.160 | 1.334 | 1.142 | -16.00 | 32.04 | 231.1 | 0.167 | 0.70 |
| SkI3 | 0.158 | 1.327 | 1.148 | -15.98 | 34.89 | 259.2 | 0.177 | 0.58 | Skz3 | 0.160 | 1.334 | 1.142 | -16.01 | 32.05 | 231.1 | 0.167 | 0.70 |
| SkI4 | 0.160 | 1.334 | 1.142 | -15.94 | 29.54 | 249.1 | 0.173 | 0.65 | Skz4 | 0.160 | 1.334 | 1.142 | -16.01 | 32.05 | 231.1 | 0.167 | 0.70 |
| SkI5 | 0.156 | 1.322 | 1.153 | -15.85 | 36.69 | 256.7 | 0.176 | 0.58 | | | | | | | | | |

give the expected results for the saturation density $n_0 \sim 0.16 \text{ fm}^{-3}$ and give the corresponding binding energy per particle $\mathcal{E}(n_0, I=0)$ as being close to -16 MeV with vanishing pressure.

The calculated values for the incompressibility modulus

$K_\infty = K(n_0, I=0)$ vary over a rather wide range from 201 MeV (SkP) to 373 MeV (SIII*) with a majority of the more modern parametrizations giving values around 230 MeV. Detailed analysis of these results can be found in Ref. [72]. Unfortunately, there is no sufficiently decisive experimental

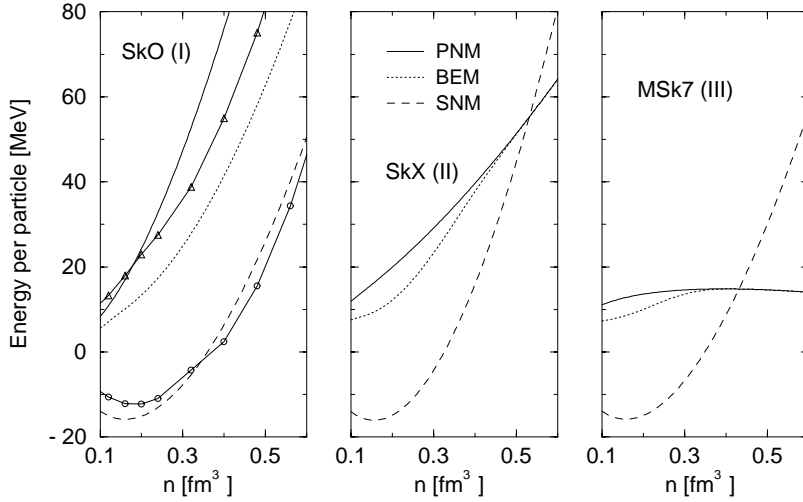


FIG. 1. The energy per particle for SNM, PNM, and BEM is plotted as a function of the baryon number density n for the SkO, SkX, and MSk7 interactions (typical representatives of groups I, II, and III). For comparison, the left-hand panel also shows equivalent curves for SNM (circles) and PNM (triangles) calculated using the “realistic” A18+ δv +UIX* potential (uncorrected) [14]. For more explanation, see text.

constraint available for this parameter. Results obtained from the analysis of data for the giant isoscalar monopole resonances are model dependent and so none of the current values, calculated with the various Skyrme potentials, can be ruled out with certainty.

Similarly, no particular conclusions can be drawn from the values for the sound speed v_s and the isoscalar effective mass m_s^* listed in Table I. They are all within expected limits with the exception of those values of m_s^*/m which are greater than unity. The models using “realistic” nucleon-nucleon potentials (see, e.g., Refs. [1,65]) and relativistic mean-field methods [20] give values of m_s^*/m between 0.6 and 0.9. Pearson and Goriely [57] argue that the values greater than unity in finite nuclei arise because of the constraint that the parametrizations should fit the ground-state masses of finite nuclei.

Some parametrizations of the Skyrme interactions have been fitted taking into account the density dependence of $\mathcal{E}(n, I)$ in infinite symmetric nuclear matter ($I=0$) and/or pure neutron matter ($I=1$) [32,41,54,55]. Again, there is no direct experimental evidence for the detailed form of these functions, especially at supernuclear densities. However the requirement of *saturation* of SNM and the fact that PNM should be *unbound* at all densities place rather strong constraints on the general trend of these functions, as already mentioned above. The condition of saturation for the SNM is satisfied for all of the Skyrme potentials (see Table I), but the density dependence of the energy per particle of PNM and BEM shows distinctly different trends for the different parameter sets. Twenty-seven of the 87 Skyrme parametrizations tested (Gs, Rs, SGI, SLy0-10, SLy230a, SV, SkI1-6, SKMP, SkO, SkO', SkT4, and SkT5—group I) predict that the energy per particle in SNM, PNM, and BEM increases with growing density beyond the saturation point with very similar gradients (Fig. 1, left panel). Some other sets, SII, SkT, SIII, SIV, SIII*, SkM, SGII, SkM*, RATP, SkT1-3, SkT6-9, SkSC2, SkSC6, SkSC10, Skyrme1', SkX, SkXce, SkXm, MSk1, MSk2, MSk5*, SKRA, Skz-1, Skz0-4 (group II) show a pattern similar to that for group I but have the energy per particle in SNM growing faster with density than in PNM and crossing the PNM curve at $\sim 3n_0$, leaving the

PNM state of matter energetically favorable above this density (Fig. 1, middle panel). The remaining Skyrme parameter sets, SI, SVI, SVII, SkP, E, Es, Z, Zs, Zs*, SkSC1, SkSC3-5, SkM1, MSk3-7, v110-v070, and BSk1 (group III) exhibit behavior similar to that of group II, with the energy per particle in SNM growing faster with increasing density than that in PNM, but the transition to PNM occurs at lower density. Also, the energy per particle in PNM here reaches a maximum (at $n=n_{PNM}^{max}$) and then decreases again with further increase of density, passing to negative values at $n=n_{PNM}^{neg}$ (Fig. 1, right panel and Table II). We note that the parametrizations SkO [53], SkX [52], and MSk7 [56] were chosen as representative for their groups because they are familiar from recent nuclear structure calculations. The variation of characteristic properties within each of the

TABLE II. Skyrme interactions predicting bound pure neutron matter (group III). Values of the baryon number density n_{PNM}^{neg} (fm^{-3}) at which the energy per particle \mathcal{E}_{PNM} (MeV) becomes negative are listed together with the maximum value of \mathcal{E}_{PNM} , \mathcal{E}_{PNM}^{max} (MeV), and the corresponding baryon number density n_{PNM}^{max} (fm^{-3}). The parameter sets are given in order of increasing values of n_{PNM}^{neg} . See text for further explanation.

| Skyrme | n_{PNM}^{neg} | \mathcal{E}_{PNM}^{max} | n_{PNM}^{max} | Skyrme | n_{PNM}^{neg} | \mathcal{E}_{PNM}^{max} | n_{PNM}^{max} |
|--------|-----------------|---------------------------|-----------------|--------|-----------------|---------------------------|-----------------|
| Z | 0.24 | 15.05 | 0.10 | SkSC1 | 0.56 | 12.97 | 0.17 |
| E | 0.28 | 14.21 | 0.11 | v090 | 0.61 | 13.60 | 0.22 |
| Es | 0.28 | 13.97 | 0.10 | SkSC3 | 0.63 | 11.91 | 0.18 |
| SkM1 | 0.28 | 13.10 | 0.09 | SkP | 0.83 | 20.69 | 0.38 |
| Zs | 0.31 | 13.76 | 0.10 | v105 | 0.90 | 13.67 | 0.26 |
| SVII | 0.34 | 12.32 | 0.12 | MSk4 | 0.93 | 13.70 | 0.26 |
| SVI | 0.37 | 12.20 | 0.12 | MSk5 | 0.98 | 13.83 | 0.28 |
| SkSC5 | 0.41 | 15.95 | 0.14 | BSk1 | 0.98 | 13.55 | 0.27 |
| v070 | 0.41 | 13.70 | 0.17 | v100 | 0.99 | 14.38 | 0.31 |
| v075 | 0.45 | 13.61 | 0.17 | MSk3 | 1.19 | 13.74 | 0.28 |
| SkSC4 | 0.49 | 13.65 | 0.16 | v110 | 1.25 | 13.73 | 0.28 |
| v080 | 0.50 | 13.60 | 0.19 | MSk7 | 1.57 | 14.84 | 0.40 |
| Zs* | 0.53 | 14.19 | 0.17 | MSk6 | 1.63 | 15.03 | 0.41 |
| SI | 0.54 | 14.39 | 0.18 | | | | |

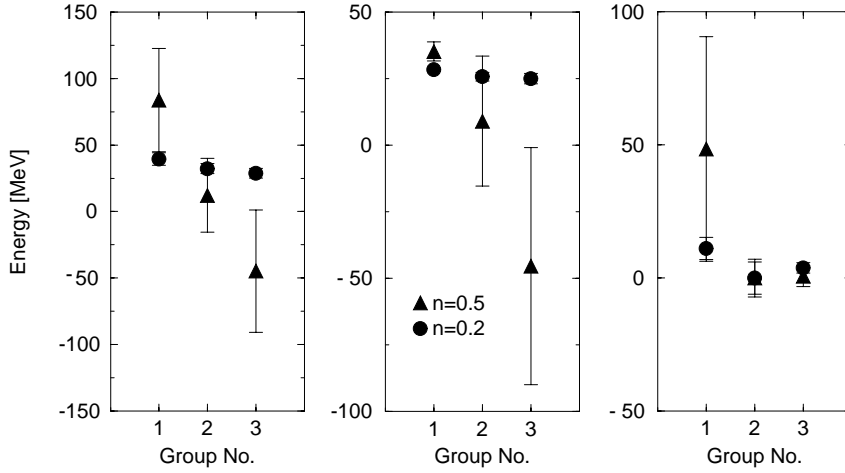


FIG. 2. Average values of $\mathcal{E}_{PNM} - \mathcal{E}_{SNM}$ (left panel), $\mathcal{E}_{BEM} - \mathcal{E}_{SNM}$ (middle panel), and $\mathcal{E}_{PNM} - \mathcal{E}_{BEM}$ (right panel) at particle number density $n=0.2$ and 0.5 fm^{-3} as calculated for parametrizations of groups I–III. See text for more explanation.

groups is shown in Fig. 2, where we show the calculated values of $\mathcal{E}_{PNM} - \mathcal{E}_{SNM}$, (left panel), $\mathcal{E}_{BEM} - \mathcal{E}_{SNM}$ (middle panel), and $\mathcal{E}_{PNM} - \mathcal{E}_{BEM}$ (right panel), representing the difference between energy per particle of PNM and SNM, BEM and SNM, and PNM and BEM, respectively, at two values of particle number density n . The errors, calculated as rms deviations from the average value, illustrate the spread within each group. We see clearly that differences between groups at density $n=0.2 \text{ fm}^{-3}$, close to nuclear saturation density n_0 , are insignificant and the spread is small. The result is very different at $n=0.5 \text{ fm}^{-3}$, about $3n_0$. The differences between groups are markedly seen, despite larger errors due to wider spread of the energy differences within a group. This is a consequence of some variation in the density dependence of calculated energies for different parametrizations within a group. The appearance of negative values of \mathcal{E}_{PNM} indicates the presence of bound PNM at higher densities, which is regarded as an unphysical result.

The density dependence of the energy per particle of the nucleon components of the BEM, \mathcal{E}_N , obviously follows a pattern which lies between the two limiting cases, SNM and PNM, for all of the parameter sets. The pressure depends on the gradient of $\mathcal{E}_N(n)$ [see Eq. (8)] and so it follows that the

parametrizations of groups II and III give lower pressures for a given density than those of group I, with those of group III even giving unphysical negative pressures at the higher densities. None of those from group III can produce neutron-star models with masses as high as the “canonical” $1.4 M_\odot$ and so they can all be excluded from consideration on those grounds. As for group II, the predicted neutron stars are smaller than those modeled using the parametrizations I, as discussed later in more detail.

The density dependence of \mathcal{E}_{SNM} and \mathcal{E}_{PNM} determines the density dependence of the asymmetry energy coefficient a_s , defined by Eqs. (11) and (12). This variable is particularly important because it depends on the isospin part of the interaction and is relevant for correctly describing nuclei with high values of isospin far from stability. At nuclear saturation density, the values given for a_s vary between 24.6 MeV (SkSC6) and 37.6 MeV (SkI1) (Ref. [72] and Table I). However, a_s cannot be measured precisely and all of these values are within the expected empirical limits (see, for example, the discussion in Refs. [1,28]). The calculated values of a_s as a function of baryon number density are illustrated in Fig. 3.

Parameter sets of group I show a monotonic increase of a_s with increasing baryon number density (Fig. 3, left panel).

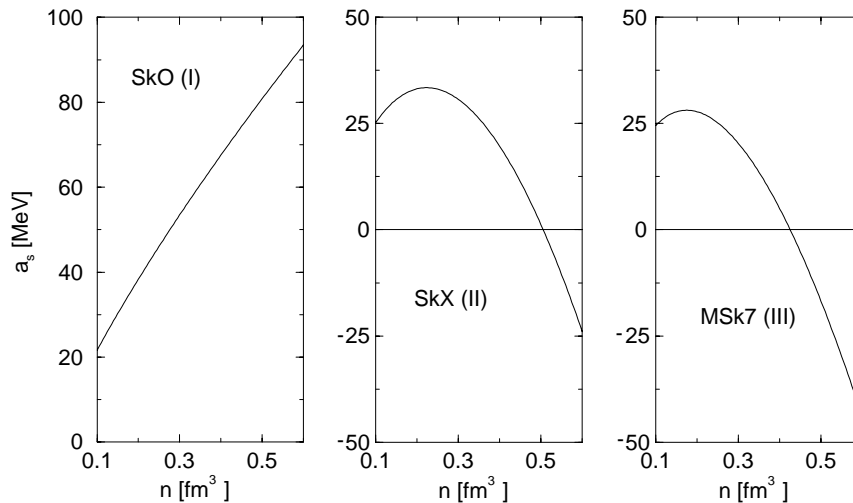


FIG. 3. The asymmetry coefficient a_s is plotted as a function of the baryon number density n for the SkO, SkX, and MSk7 interactions. See text for more explanation.

TABLE III. Skyrme interaction parametrizations which predict that the asymmetry energy coefficient a_s (MeV) decreases with increasing baryon number density n (fm^{-3}) beyond some threshold density (groups II and III). The parameter sets are ordered according to increasing values of the density at which a_s becomes negative $n_{a_s}^{neg}$. See text for further explanation.

| Skyrme | $n_{a_s}^{neg}$ | a_s^{max} | $n_{a_s}^{max}$ | Skyrme | $n_{a_s}^{neg}$ | a_s^{max} | $n_{a_s}^{max}$ |
|--------|-----------------|-------------|-----------------|----------|-----------------|-------------|-----------------|
| Z | 0.27 | 28.67 | 0.12 | SkSC2 | 0.46 | 25.02 | 0.19 |
| SVI | 0.28 | 26.94 | 0.14 | SkSC6 | 0.46 | 24.86 | 0.19 |
| SVII | 0.28 | 27.07 | 0.14 | Skyrme1' | 0.47 | 31.82 | 0.22 |
| E | 0.29 | 28.51 | 0.14 | SkP | 0.48 | 30.77 | 0.20 |
| Es | 0.31 | 27.86 | 0.12 | SII | 0.49 | 38.97 | 0.23 |
| SkM1 | 0.31 | 26.69 | 0.12 | Skz2 | 0.50 | 32.61 | 0.19 |
| SIII | 0.32 | 28.29 | 0.16 | SkX | 0.51 | 33.43 | 0.22 |
| SI | 0.32 | 29.25 | 0.16 | SkXce | 0.52 | 32.66 | 0.22 |
| Zs | 0.32 | 27.73 | 0.13 | Skz4 | 0.53 | 32.12 | 0.17 |
| v070 | 0.35 | 28.02 | 0.16 | Skz3 | 0.54 | 32.42 | 0.19 |
| v075 | 0.37 | 28.00 | 0.16 | SkXm | 0.54 | 33.49 | 0.23 |
| SkSC5 | 0.37 | 31.06 | 0.15 | SkSC10 | 0.55 | 23.99 | 0.22 |
| v080 | 0.38 | 28.01 | 0.16 | Skz0 | 0.55 | 34.75 | 0.24 |
| SIII* | 0.38 | 33.84 | 0.19 | Skz1 | 0.55 | 33.74 | 0.22 |
| SkSC4 | 0.38 | 28.82 | 0.16 | SKT7 | 0.59 | 32.08 | 0.25 |
| Zs* | 0.38 | 28.85 | 0.16 | SKT6 | 0.60 | 32.49 | 0.25 |
| v090 | 0.40 | 28.05 | 0.17 | MSk1 | 0.62 | 33.28 | 0.25 |
| SkSC1 | 0.40 | 28.11 | 0.16 | MSk2 | 0.62 | 33.10 | 0.25 |
| SkSC3 | 0.40 | 27.02 | 0.16 | RATP | 0.64 | 32.40 | 0.26 |
| Bsk1 | 0.41 | 27.92 | 0.17 | SKT8 | 0.69 | 33.48 | 0.27 |
| SKT | 0.41 | 26.60 | 0.20 | SKT9 | 0.69 | 33.36 | 0.27 |
| MSk3 | 0.41 | 28.09 | 0.17 | Skz-1 | 0.71 | 40.80 | 0.32 |
| MSk4 | 0.41 | 28.11 | 0.17 | SIV | 0.77 | 46.76 | 0.38 |
| MSk5* | 0.41 | 28.09 | 0.17 | SGII | 0.78 | 32.70 | 0.32 |
| v105 | 0.41 | 28.10 | 0.17 | SkM* | 0.83 | 38.22 | 0.35 |
| v100 | 0.42 | 28.15 | 0.17 | SkM | 0.92 | 41.02 | 0.38 |
| v110 | 0.42 | 28.12 | 0.17 | SKRA | 1.02 | 44.51 | 0.43 |
| MSk5 | 0.42 | 28.12 | 0.17 | SKT1 | 1.19 | 48.19 | 0.48 |
| MSk7 | 0.43 | 28.13 | 0.17 | SKT2 | 1.19 | 48.19 | 0.49 |
| MSk6 | 0.43 | 28.19 | 0.17 | SKT3 | 1.20 | 47.55 | 0.49 |

Sets belonging to groups II and III show a distinctly different behavior [Fig. 3, middle (II) and right (III) panels—note the change of the vertical scale]: a_s reaches a maximum value at a baryon number density $n_{a_s}^{max}$ and then decreases with increasing n until it becomes negative at the densities $n_{a_s}^{neg}$ listed in Table III. The difference between the predictions for a_s from groups II and III is in that those from group III typically give a_s reaching negative values at lower densities than for those of group II.

The nuclear symmetry energy is directly related to the proton fraction y_p in BEM through Eq. (17) and this quantity has an important significance for astrophysics. If $\mathcal{S}(n)$ increases steadily with increasing density, this implies also an increasing proton fraction, whereas the opposite behavior leads to a transition to pure neutron matter at high densities. The proton concentration in BEM affects the cooling of neutron stars [73], as well as the conditions for the creation of heavy mesons, hyperons, and possible hadron-quark or pure quark phases. It also influences the mass-radius relation for neutron-star models (see, e.g., Refs. [74,75]). We emphasize that the density dependence of the nuclear symmetry energy at supranuclear densities is the key feature which divides the Skyrme parametrizations into two main classes. The first class contains group I, which has a growing proton fraction with increasing density in the stellar matter, while the second class contains groups II and III, which predict a transition to pure neutron matter at higher densities.

For determining the particle composition of BEM, it is first necessary to calculate the chemical potentials and the results for these are shown in Fig. 4. For the parameter sets of group I, the neutron and proton chemical potentials increase monotonically with increasing density. The difference $\mu_n - \mu_p = \mu_e = \mu_\mu$ remains positive and grows with increasing density in the region $0.1 \leq n \leq 0.5 \text{ fm}^{-3}$, indicating an increasing proton fraction and correspondingly increasing numbers of electrons and muons (Fig. 4, left panels).

A quite different behavior is seen for the parameter sets of groups II and III. For group II, both μ_n and μ_p increase with increasing density, but μ_p grows faster than μ_n in such a

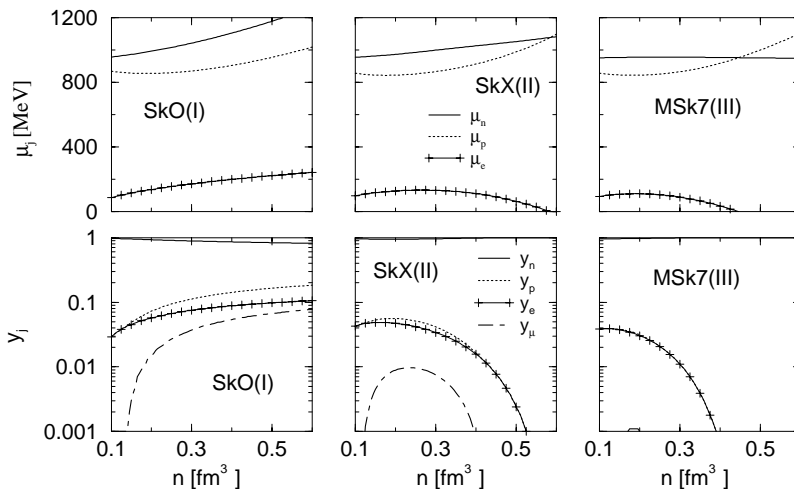


FIG. 4. Chemical potential and particle composition of BEM for the SkO, SkX, and MSK7 interactions. See text for more explanation.

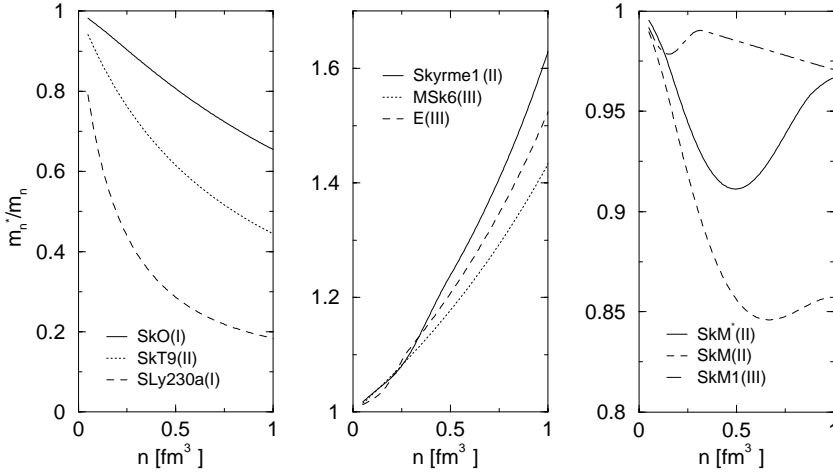


FIG. 5. Neutron effective mass as a function of density for selected Skyrme interactions. Examples have been chosen to show the spread and variety of the predicted density dependence of m_n^* for different parametrizations.

way that the difference $\mu_n - \mu_p$ reaches a maximum and then starts to decrease again. The electron chemical potential μ_e (equal to $\mu_n - \mu_p$ in β -equilibrium) soon falls below the rest mass of the muon thus forbidding generation of muons. Eventually $\mu_n - \mu_p$ becomes equal to zero (at a density n_{thr}) and then becomes negative, implying that no electrons and protons can be present at densities greater than or equal to n_{thr} . It follows that the “ β -equilibrium” phase stops here and there is a transition to pure neutron matter (Fig. 4, central panels). This often occurs at densities around $(2-3)n_0$. The density dependence of μ_n and μ_p predicted by parametrizations of group III is similar to that of group II except that μ_n reaches a maximum value at rather low densities (less than 0.3 fm^{-3}) and then starts to fall again as the density increases further. This behavior is not what is expected if μ_n is taken to be the zero-temperature chemical potential (Fermi energy) for an equilibrium system of fermions, which should rise with increasing density [76]. For noninteracting fermions, the chemical potential is related to density as $\propto n^{2/3}$ and is inversely proportional to the effective mass of the particle which is believed to decrease with increasing density (as predicted by the realistic potentials and RMF models [77]). Thus the decrease of chemical potential with increasing density can be caused either by the contribution from the fermion-fermion interaction or by an anomalous density dependence of the fermion effective mass.

In this context, it is instructive to examine the predictions of various Skyrme potentials for the density dependence of the neutron mass in a dense medium using relation (13). We show results for this in Fig. 5. All parametrizations of group I and the majority of group II show nonincreasing neutron effective mass with increasing density (see Fig. 5, left panel) as predicted by other model calculations [20,75,77]. There are two subfamilies of parameter sets SkSC1-6,10 [groups III (SkSC 1,3-5) and II (SkSC 2,6,10)] and SkT1-6 [groups II (SkT 1-3,6) and I (SkT 4,5)] for which the effective mass remains constant.

Most of the sets of group III (BSk1, E, Es, SI, SVI, MSk3-7, v100, v105, and v110) and some of those of group II (SkT7, MSk1-2) give increasing neutron mass with increasing density (Fig. 5, central panel). The parametrization SkMS shows the neutron mass decreasing with density up to

0.5 fm^{-3} but then subsequently increasing again, and sets Z, Zs, Zs*, and SkM1 give m_n^* reaching a local minimum at $n \sim 0.15 \text{ fm}^{-3}$ and then temporarily rising again before resuming its decreasing behavior at the highest densities (Fig. 5, right panel).

An unexpected constraint on some of the Skyrme parameters comes from requiring that the predictions for the neutron effective mass should not exhibit unphysical singularities (see Fig. 6 for examples of these). Using Eq. (13), it can be shown that such singularities will arise if

$$2\Theta_v I - \Theta_s(1+I) = \frac{8\hbar^2}{nm} \quad (24)$$

at some density n , where Θ_v and Θ_s are quantities which are expressed in terms of the Skyrme parameters by $\Theta_v = t_1(2 + x_1) + t_2(2 + x_2)$ and $\Theta_s = 3t_1 + (5 + 4x_2)t_2$ [23,60]. There are 13 parameter sets for which such a singularity can occur: v070 (0.30), v075 (0.37), v080 (0.46), SkXce (0.46), SkP (0.47), SkX (0.49), SkXm (0.60), v090 (0.76), Skz-1 (0.79), SVII(0.84), Skz0 (1.12), SVI (1.16), and v100 (1.65), the number in parentheses giving the critical baryon number density at which the singularity occurs (in fm^{-3}). Although some of these critical densities are considerably higher than

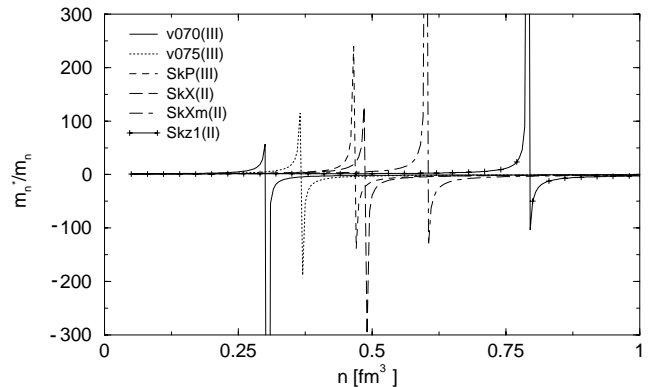


FIG. 6. Anomalous dependence of the neutron effective mass on baryon number density as predicted by some Skyrme interactions. For more explanation, see text.

TABLE IV. The proton fraction y_p in β -stable $n+p+e+\mu$ matter as predicted by Skyrme parametrizations from groups II and III. The baryon number density n_{thr} at which the transition to pure neutron matter occurs, the maximum proton fraction y_p^{max} (reached at density $n_{y_p}^{max}$), and the estimated threshold densities for the creation of muons, Σ^- and Λ hyperons are all listed. All of the densities are measured in units of fm^{-3} . See text for more details.

| Skyrme | n_{thr} | y_p^{max} | $n_{y_p}^{max}$ | n_μ | n_{Σ^-} | n_Λ | Skyrme | n_{thr} | y_p^{max} | $n_{y_p}^{max}$ | n_μ | n_{Σ^-} | n_Λ |
|----------|-----------|-------------|-----------------|---------|----------------|-------------|--------|-----------|-------------|-----------------|---------|----------------|-------------|
| SII | 0.56 | 0.079 | 0.21 | 0.10 | 0.31 | 0.41 | SkM* | 1.11 | 0.064 | 0.29 | 0.13 | 0.38 | 0.55 |
| SkT8 | 0.74 | 0.048 | 0.21 | 0.13 | 0.58 | 0.60 | SIV | 1.11 | 0.101 | 0.35 | 0.12 | 0.27 | 0.36 |
| SkT9 | 0.75 | 0.047 | 0.21 | 0.13 | 0.57 | 0.60 | SkT1 | 1.22 | 0.077 | 0.35 | 0.12 | 0.34 | 0.48 |
| RATP | 0.87 | 0.052 | 0.22 | 0.12 | 0.46 | 0.57 | SkT2 | 1.22 | 0.078 | 0.36 | 0.12 | 0.34 | 0.48 |
| SGII | 1.03 | 0.047 | 0.28 | 0.15 | 0.43 | 0.57 | SkT3 | 1.22 | 0.074 | 0.35 | 0.13 | 0.34 | 0.48 |
| Skz-1 | 1.04 | 0.084 | 0.31 | 0.12 | 0.35 | 0.54 | SkM | 1.23 | 0.071 | 0.32 | 0.12 | 0.46 | 0.53 |
| SKRA | 1.50 | 0.081 | 0.37 | 0.12 | 0.34 | 0.50 | | | | | | | |
| SIII | 0.34 | 0.044 | 0.13 | 0.12 | | 1.38 | SkX | 0.56 | 0.056 | 0.19 | 0.12 | | 0.70 |
| SIII* | 0.40 | 0.060 | 0.16 | 0.10 | | 0.68 | Skz2 | 0.58 | 0.057 | 0.16 | 0.10 | | 0.88 |
| SkSC2 | 0.47 | 0.030 | 0.12 | | | 1.11 | SkXce | 0.58 | 0.053 | 0.19 | 0.12 | | 0.66 |
| SkSC6 | 0.47 | 0.029 | 0.12 | | | 1.08 | SkT6 | 0.61 | 0.046 | 0.19 | 0.13 | | 0.75 |
| SkT | 0.47 | 0.035 | 0.19 | 0.16 | | 0.47 | MSk2 | 0.62 | 0.047 | 0.19 | 0.13 | | 0.72 |
| Skyrme1' | 0.49 | 0.048 | 0.20 | 0.14 | | 0.43 | MSk1 | 0.63 | 0.047 | 0.20 | 0.13 | | 0.68 |
| Skz4 | 0.50 | 0.054 | 0.12 | 0.10 | | 0.69 | SkT7 | 0.68 | 0.048 | 0.20 | 0.13 | | 0.71 |
| Skz3 | 0.56 | 0.054 | 0.14 | 0.10 | | 0.72 | Skz1 | 0.68 | 0.060 | 0.19 | 0.11 | | 0.83 |
| SkSC10 | 0.56 | 0.023 | 0.15 | | | 0.71 | Skz0 | 0.74 | 0.066 | 0.21 | 0.11 | | 1.09 |
| Z | 0.28 | 0.051 | 0.09 | 0.10 | | | v080 | 0.41 | 0.043 | 0.12 | 0.12 | | |
| SVI | 0.29 | 0.042 | 0.10 | 0.13 | | | BSk1 | 0.41 | 0.039 | 0.11 | 0.14 | | |
| SVII | 0.29 | 0.043 | 0.10 | 0.12 | | | MSk4 | 0.41 | 0.040 | 0.12 | 0.14 | | |
| E | 0.30 | 0.049 | 0.10 | 0.11 | | | v090 | 0.41 | 0.041 | 0.12 | 0.13 | | |
| Es | 0.32 | 0.049 | 0.09 | 0.11 | | | v105 | 0.41 | 0.040 | 0.11 | 0.14 | | |
| SkM1 | 0.33 | 0.047 | 0.08 | 0.12 | | | v110 | 0.41 | 0.039 | 0.12 | 0.14 | | |
| SI | 0.34 | 0.046 | 0.14 | 0.12 | | | MSk3 | 0.42 | 0.040 | 0.11 | 0.14 | | |
| Zs | 0.34 | 0.048 | 0.09 | 0.11 | | | MSk5 | 0.42 | 0.040 | 0.12 | 0.14 | | |
| SkSC5 | 0.38 | 0.054 | 0.12 | 0.10 | | | Zs* | 0.43 | 0.047 | 0.12 | 0.12 | | |
| SkSC4 | 0.39 | 0.044 | 0.10 | 0.12 | | | v100 | 0.43 | 0.040 | 0.12 | 0.14 | | |
| v070 | 0.39 | 0.045 | 0.12 | 0.12 | | | MSk6 | 0.43 | 0.040 | 0.12 | 0.14 | | |
| v075 | 0.40 | 0.044 | 0.12 | 0.12 | | | MSk7 | 0.43 | 0.039 | 0.12 | 0.14 | | |
| SkSC1 | 0.40 | 0.041 | 0.11 | 0.12 | | | SkP | 0.54 | 0.049 | 0.17 | 0.12 | | |
| SkSC3 | 0.40 | 0.038 | 0.11 | 0.14 | | | MSk5* | 0.44 | 0.042 | 0.12 | 0.12 | | |
| SkXm | 0.60 | 0.055 | 0.19 | 0.12 | | | | | | | | | |

the central density expected in the most massive stable neutron stars, at least half of them are in the region of densities $n < 3n_0$.

Returning to the question of the composition of neutron-star matter at supranuclear densities, we repeat that the presence of protons (and, consequently, of e^- or $e^- + \mu^-$) may be rather important for modeling the composition of neutron-star matter at densities higher than $\sim (2-3)n_0$. This problem was discussed at length in our previous paper [28]. At sufficiently high densities, one expects that heavy baryons and mesons will appear in addition to the particles which we have been considering so far, but it can be questioned how great an effect these will have on the EOS itself. In the past, some calculations have been performed for pure neutron matter (e.g., Refs. [63,78]) and it was found that, apart from the EOS obtained being slightly stiffer than that for the multicomponent matter, the inclusion of protons, leptons, and hyperons in the calculation made very little difference. Similarly, an extrapolated BEM EOS has been found to differ

only slightly from one including hyperons [14,23]. However, this may happen only because the hyperon-hyperon and hyperon-nucleon potentials used at present are taken to be similar to those of nucleons. The true form of these potentials is still rather poorly known, although some progress is being made on this (see, e.g., Refs. [8,9]). Should future studies find a significant difference between the hyperonic and nucleonic potentials then the EOS could change dramatically [79].

The contributions of heavy mesons and hyperons to the total energy of dense matter are not included in the present work and so we cannot calculate the equilibrium composition of such matter as a function of density. An estimate of the threshold densities for appearance of hyperons can be made, however. The baryon chemical potential μ_B is expressed in terms of two independent chemical potentials μ_n and μ_e as [80]

$$\mu_B = \mu_n - q_B^{el} \mu_e, \tag{25}$$

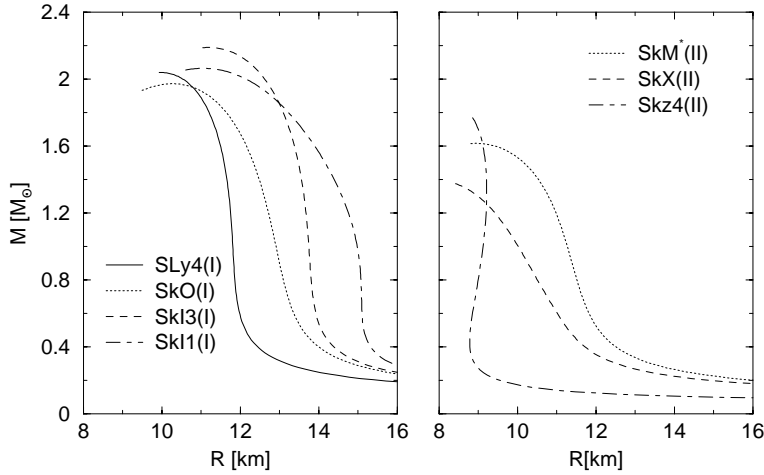


FIG. 7. The gravitational masses of nonrotating neutron-star models (measured in solar masses) plotted against radius (in kilometers), calculated for β -stable nucleon+lepton matter using selected Skyrme interactions of group I (left panel) and group II (right panel), supplemented by the BPS EOS at low densities.

where q_B^{el} is the electric charge of the baryon. The first appearance of particle B in chemically equilibrated matter occurs at the density at which μ_B exceeds the lowest energy state of B in the medium. We use Eq. (25) assuming that for hyperons μ_B is equal to the vacuum rest mass (neglecting hyperon-hyperon interactions and the density dependence of the hyperon effective mass). Also, reactions yielding heavy mesons are not taken into consideration because weak, strangeness nonconserving interactions are assumed to dominate in the cold neutron-star matter [20].

The Skyrme parametrizations of group I (with growing proton fraction y_p as a function of density) should behave at higher densities in essentially the same way as predicted by “realistic” potentials [1] or RMF [77] models. The average threshold densities for the creation of Σ^- , Λ , Σ^0 , and Σ^+ hyperons are $0.29 \pm 0.04 \text{ fm}^{-3}$, $0.41 \pm 0.04 \text{ fm}^{-3}$, $0.50 \pm 0.05 \text{ fm}^{-3}$, and $0.74 \pm 0.06 \text{ fm}^{-3}$, respectively. The thresholds for Σ^- and Λ can be compared to the values 0.34 fm^{-3} and 0.47 fm^{-3} calculated with A18+ δv +UIX* [14].

In Table IV, we list the threshold densities for the creation of Σ^- and Λ hyperons as predicted by parametrizations of groups II and III. For the parameter sets listed in the top part of the table, the transition to pure neutron matter occurs at rather high densities [(3.5–9.3) n_0] and both thresholds lie at lower densities where protons are still present. These models are most likely to give particle compositions similar to those given by the parameter sets of group I. If the transition to pure neutron matter occurs at rather low densities (the middle part of Table IV), the creation of Σ^- is forbidden by the requirement of charge conservation. (Possible reactions such as $n+n \rightarrow \Sigma^-+p$ will not proceed because $2\mu_n - \mu_p$ is smaller than μ_{Σ^-} .) The first hyperon to appear is then Λ and an equilibrium can be established for $n+n \leftrightarrow \Lambda+n$. Finally, parametrizations listed in the bottom part of Table IV (mostly of group III) do not predict the appearance of either Σ^- or Λ hyperons in the relevant density range. Because a nonrelativistic approach is being used in this work, one should check on whether the calculated speed of sound v_s may become higher than the speed of light c at high densities. We

note that none of the parametrizations considered here reaches this limit in the region of particle number densities $(1-5)n_0$.

We turn now to the properties of related neutron-star models, concentrating mainly on ones with the canonical mass, $1.4M_\odot$. As discussed in Sec. II above, these models can be calculated using the EOS for BEM matched on to the BPS EOS at lower densities. We have already mentioned that the behavior of pressure at high densities predicted for BEM by Skyrme parameter sets of group III does not allow nonrotating equilibrium neutron-star models with masses as high as $1.4M_\odot$ and these parametrizations are therefore excluded. In contrast, all 27 parameter sets of group I give neutron-star models with mass–radius relations which do not contradict present observational data, as illustrated in Fig. 7 (left panel) and Table V. The radii and central particle number densities for the $1.4M_\odot$ models lie in the ranges $12.5 \pm 0.9 \text{ km}$ and $0.48 \pm 0.07 \text{ fm}^{-3}$, respectively. If the EOS for the BEM is extrapolated up to densities above 0.5 fm^{-3} , the maximum gravitational mass for these parametrizations is then calculated to be $2.07 \pm 0.10M_\odot$ with radii of $10.4 \pm 0.5 \text{ km}$ and central densities of $1.12 \pm 0.02 \text{ fm}^{-3}$. When observational constraints on the radius of neutron stars become known more precisely (e.g., to within an uncertainty of less than 1 km, as suggested recently [81]), more selection among these models will then become possible.

As pointed out above, neutron-star models calculated with Skyrme interactions of group II are systematically smaller than those for group I due to the slower increase in pressure with increasing density. Ten out of 33 models from group II (those based on the interactions MSk5*, SIII, SIII*, SkSC2, SkSC6, SkX, SkXm, Skz0, Skz1, and Skz-1) do not reach the canonical mass of $1.4M_\odot$ and are hence excluded. The remaining ones give $1.4M_\odot$ models with radii of $10 \pm 1 \text{ km}$ and central number densities of $1.0 \pm 0.4 \text{ fm}^{-3}$. Extrapolated EOS’s for BEM with these parametrizations give maximum-mass models with $M = 1.7 \pm 0.2M_\odot$ having radii of $9 \pm 1 \text{ km}$ and central densities of $1.7 \pm 0.4 \text{ fm}^{-3}$. Some representative mass-radius relations for group II are plotted in Fig. 7 (right panel); these show a notable difference from the equivalent curves for group I. The hope is that, rather soon,

TABLE V. Parameters of $1.4M_{\odot}$ neutron-star models: n_c and ρ_c are the central number density (fm^{-3}) and mass density ($10^{15} \text{ g cm}^{-3}$), respectively, R (km) is the radius, A (10^{57}) is the total baryon number, E_{bind} (10^{53} ergs) is the binding energy, and τ (msec) is the estimate of the rotation period calculated from Eq. (23).

| Skyrme | n_c | ρ_c | R | A | E_{bind} | τ |
|---------|-------|----------|-------|------|------------|--------|
| Gs | 0.42 | 0.77 | 13.25 | 1.83 | 2.25 | 1.05 |
| Rs | 0.43 | 0.80 | 13.04 | 1.85 | 2.32 | 1.03 |
| SGI | 0.41 | 0.74 | 12.93 | 1.83 | 2.36 | 1.02 |
| SV | 0.34 | 0.61 | 13.84 | 1.81 | 2.12 | 1.13 |
| SLy0 | 0.54 | 1.00 | 11.67 | 1.86 | 2.60 | 0.87 |
| SLy1 | 0.54 | 1.00 | 11.67 | 1.86 | 2.60 | 0.87 |
| SLy2 | 0.54 | 1.00 | 11.68 | 1.86 | 2.61 | 0.87 |
| SLy3 | 0.55 | 1.02 | 11.59 | 1.86 | 2.62 | 0.86 |
| SLy4 | 0.55 | 1.00 | 11.65 | 1.87 | 2.62 | 0.87 |
| SLy5 | 0.54 | 1.00 | 11.70 | 1.88 | 2.65 | 0.87 |
| SLy6 | 0.53 | 0.98 | 11.76 | 1.86 | 2.58 | 0.88 |
| SLy7 | 0.53 | 0.98 | 11.76 | 1.87 | 2.61 | 0.88 |
| SLy8 | 0.54 | 1.00 | 11.68 | 1.87 | 2.63 | 0.87 |
| SLy9 | 0.46 | 0.83 | 12.42 | 1.84 | 2.40 | 0.96 |
| SLy10 | 0.56 | 1.03 | 11.48 | 1.85 | 2.63 | 0.85 |
| SLy230a | 0.52 | 0.95 | 11.78 | 1.88 | 2.66 | 0.88 |
| SkI1 | 0.37 | 0.67 | 14.37 | 1.83 | 2.08 | 1.19 |
| SkI2 | 0.39 | 0.72 | 13.58 | 1.84 | 2.21 | 1.09 |
| SkI3 | 0.37 | 0.68 | 13.56 | 1.83 | 2.18 | 1.09 |
| SkI4 | 0.44 | 0.80 | 12.56 | 1.83 | 2.43 | 0.98 |
| SkI5 | 0.35 | 0.64 | 14.13 | 1.81 | 2.05 | 1.16 |
| SkI6 | 0.44 | 0.80 | 12.55 | 1.86 | 2.49 | 0.97 |
| SkMP | 0.47 | 0.86 | 12.62 | 1.86 | 2.44 | 0.98 |
| SkO | 0.50 | 0.93 | 12.46 | 1.86 | 2.42 | 0.96 |
| SkO' | 0.53 | 0.98 | 12.12 | 1.84 | 2.43 | 0.92 |
| SkT4 | 0.46 | 0.85 | 12.87 | 1.85 | 2.27 | 1.01 |
| SkT5 | 0.58 | 1.09 | 12.20 | 1.85 | 2.31 | 0.93 |

TABLE VI. Critical threshold densities n_{URCA} for the direct URCA process to occur together with the corresponding gravitational mass M_{URCA} ; also listed are the corresponding quantities for the maximum-mass model, n_{max} and M_{max} (calculated with the extrapolated EOS). Densities are given in fm^{-3} and masses in units of M_{\odot} . For more explanation, see text.

| Skyrme | n_{URCA} | M_{URCA} | n_{max} | M_{max} |
|---------|------------|------------|-----------|-----------|
| Gs | 0.29 | 0.94 | 1.07 | 2.08 |
| Rs | 0.33 | 1.03 | 1.08 | 2.08 |
| SGI | 0.49 | 1.67 | 1.01 | 2.22 |
| SV | 0.26 | 0.95 | 0.80 | 2.38 |
| SLy0 | 1.34 | | 1.20 | 2.04 |
| SLy1 | 1.34 | | 1.20 | 2.04 |
| SLy2 | 1.30 | | 1.20 | 2.04 |
| SLy3 | 1.53 | | 1.21 | 2.03 |
| SLy4 | 1.42 | | 1.20 | 2.04 |
| SLy5 | 1.23 | | 1.20 | 2.04 |
| SLy6 | 1.18 | 2.05 | 1.19 | 2.05 |
| SLy7 | 1.20 | | 1.18 | 2.06 |
| SLy8 | 1.31 | | 1.20 | 2.04 |
| SLy9 | 0.59 | 1.52 | 1.20 | 2.04 |
| SLy10 | | | 1.17 | 2.04 |
| SLy230a | 0.83 | 1.99 | 1.15 | 2.08 |
| SkI1 | 0.21 | 0.88 | 1.05 | 2.07 |
| SkI2 | 0.27 | 0.92 | 1.03 | 2.11 |
| SkI3 | 0.26 | 0.90 | 0.98 | 2.19 |
| SkI4 | 0.50 | 1.59 | 1.00 | 2.15 |
| SkI5 | 0.22 | 0.86 | 0.97 | 2.18 |
| SkI6 | 0.51 | 1.61 | 1.04 | 2.16 |
| SkMP | 0.43 | 1.29 | 1.11 | 2.08 |
| SkO | 0.38 | 1.06 | 1.19 | 1.97 |
| SkO' | 0.58 | 1.49 | 1.23 | 1.95 |
| SkT4 | 0.29 | 0.85 | 1.12 | 2.03 |
| SkT5 | 0.28 | 0.73 | 1.32 | 1.82 |

observations will be able to place much tighter limits on the mass-radius curve for neutron stars (gravitational wave observations of coalescing neutron-star binaries may be particularly useful for this [82]). The observations could then give stringent new constraints for the EOS of neutron-star matter and the results presented in this paper are ready to be compared.

The issue of neutron-star cooling mechanisms can, in principle, place further important constraints on neutron-star models. However, as mentioned briefly above and discussed in more detail previously [28], the cooling processes for both young and old neutron-stars are not currently known with any certainty, although several scenarios exist [73,74,83–85]. We explore here the possible relevance of the direct URCA processes given by

$$n \rightarrow p + l + \bar{\nu}_l, \quad p + l \rightarrow n + \nu_l, \quad (26)$$

(where l stands for the leptons being considered here—electrons and muons) within the context of the Skyrme parametrizations studied in this paper. For this direct URCA

process to take place, the relative components of the BEM must satisfy the appropriate conditions for conservation of energy and momentum: $y_n^{1/3} < y_p^{1/3} + y_e^{1/3}$ and $y_n^{1/3} < y_p^{1/3} + y_{\mu}^{1/3}$. It has been argued that this will be satisfied only at densities n several times larger than the nuclear saturation density $n_0 = 0.16 \text{ fm}^{-3}$ [73,83,84] when the proton fraction in BEM reaches a threshold value of $\sim 14\%$. It follows from Eq. (18) that the steeper the increase of the symmetry energy with increasing number density, the faster will be the growth of the proton fraction y_p . It is therefore not surprising that almost all of the parametrizations of group I (with the single exception of SLy10) *do* satisfy these conditions for astrophysically interesting models of sufficiently high mass, whereas this does not happen for any of the parametrizations of group II. (We recall that only models with central densities below that of the maximum-mass model represent stable configurations of astrophysical interest.) As can be seen in Table VI, the critical threshold density for the URCA process to take place turns out to be rather low: $(2-3)n_0$ which is usually below the central density of the $1.4M_{\odot}$ model. The exceptions to this pattern are the parametrizations of the SLy

TABLE VII. Parameters of the recommended Skyrme parametrizations. The values given here are for illustrative purposes and are quoted to restricted accuracy (see text); values with the full accuracy can be found in the original references (see Sec. II).

| Skyrme | t_0 | t_1 | t_2 | t_3 | x_0 | x_1 | x_2 | x_3 | α | K_∞ | (m_s^*/m) | (m_v^*/m) |
|---------|---------|-------|--------|-------|-------|-------|-------|-------|----------|------------|-------------|-------------|
| Gs | -1800.2 | 336.2 | -85.7 | 11113 | -0.49 | 0.00 | 0.00 | -1.03 | 0.30 | 237.6 | 0.78 | 0.68 |
| Rs | -1798.0 | 336.0 | -84.8 | 11083 | -0.40 | 0.00 | 0.00 | -0.87 | 0.30 | 237.7 | 0.78 | 0.68 |
| S GI | -1603.0 | 515.9 | 84.5 | 8000 | -0.02 | -0.50 | -1.73 | 0.14 | 0.33 | 262.1 | 0.61 | 0.57 |
| SLy0 | -2486.4 | 485.2 | -440.5 | 13783 | 0.79 | -0.50 | -0.93 | 1.29 | 0.17 | 230.2 | 0.70 | 0.80 |
| SLy1 | -2487.6 | 488.3 | -568.9 | 13791 | 0.80 | -0.31 | -1.00 | 1.29 | 0.17 | 230.3 | 0.70 | 0.80 |
| SLy10 | -2506.8 | 431.0 | -305.0 | 13826 | 1.04 | -0.67 | -1.00 | 1.68 | 0.17 | 230.1 | 0.68 | 0.80 |
| SLy2 | -2484.2 | 482.2 | -290.0 | 13763 | 0.79 | -0.73 | -0.78 | 1.28 | 0.17 | 230.4 | 0.70 | 0.80 |
| SLy230a | -2490.2 | 489.5 | -566.6 | 13803 | 1.13 | -0.84 | -1.00 | 1.92 | 0.17 | 230.4 | 0.70 | 1.00 |
| SLy3 | -2481.1 | 481.0 | -540.8 | 13731 | 0.84 | -0.34 | -1.00 | 1.36 | 0.17 | 230.4 | 0.70 | 0.80 |
| SLy4 | -2488.9 | 486.8 | -546.4 | 13777 | 0.83 | -0.34 | -1.00 | 1.35 | 0.17 | 230.4 | 0.69 | 0.80 |
| SLy5 | -2483.4 | 484.2 | -556.7 | 13757 | 0.78 | -0.32 | -1.00 | 1.26 | 0.17 | 230.4 | 0.70 | 0.80 |
| SLy6 | -2479.5 | 462.2 | -448.6 | 13673 | 0.82 | -0.47 | -1.00 | 1.36 | 0.17 | 230.3 | 0.69 | 0.80 |
| SLy7 | -2480.8 | 461.3 | -433.9 | 13669 | 0.85 | -0.49 | -1.00 | 1.39 | 0.17 | 230.2 | 0.69 | 0.80 |
| SLy8 | -2481.4 | 480.8 | -538.3 | 13731 | 0.80 | -0.34 | -1.00 | 1.31 | 0.17 | 230.4 | 0.70 | 0.80 |
| SLy9 | -2511.1 | 510.6 | -429.8 | 13716 | 0.80 | -0.62 | -1.00 | 1.37 | 0.17 | 230.1 | 0.67 | 0.80 |
| SV | -1248.3 | 970.6 | 107.2 | 0 | -0.17 | 0.00 | 0.00 | 1.00 | 1.00 | 306.2 | 0.38 | 0.33 |
| SkI1 | -1913.6 | 439.8 | 2697.6 | 10592 | -0.95 | -5.78 | -1.29 | -1.56 | 0.25 | 243.2 | 0.69 | 0.80 |
| SkI2 | -1915.4 | 438.4 | 305.4 | 10548 | -0.21 | -1.74 | -1.53 | -0.18 | 0.25 | 241.3 | 0.68 | 0.80 |
| SkI3 | -1762.9 | 561.6 | -227.1 | 8106 | 0.31 | -1.17 | -1.09 | 1.29 | 0.25 | 258.7 | 0.58 | 0.80 |
| SkI4 | -1855.8 | 473.8 | 1006.9 | 9703 | 0.41 | -2.89 | -1.33 | 1.15 | 0.25 | 248.4 | 0.65 | 0.80 |
| SkI5 | -1772.9 | 550.8 | -126.7 | 8206 | -0.12 | -1.31 | -1.05 | 0.34 | 0.25 | 256.2 | 0.58 | 0.80 |
| SkI6 | -1849.3 | 483.9 | 528.4 | 9553 | 0.49 | -2.14 | -1.38 | 1.34 | 0.25 | 249.0 | 0.64 | 0.80 |
| SkMP | -2372.2 | 503.6 | 57.3 | 12585 | -0.16 | -0.40 | -2.96 | -0.27 | 0.17 | 231.3 | 0.65 | 0.58 |
| SkO | -2103.7 | 303.4 | 791.7 | 13553 | -0.21 | -2.81 | -1.46 | -0.43 | 0.25 | 223.7 | 0.90 | 0.85 |
| SkO' | -2099.4 | 301.5 | 154.8 | 13526 | -0.03 | -1.33 | -2.32 | -0.15 | 0.25 | 222.7 | 0.90 | 0.87 |
| SkT4 | -1808.8 | 303.4 | -303.4 | 12980 | -0.18 | -0.50 | -0.50 | -0.50 | 0.33 | 235.8 | 1.00 | 1.00 |
| SkT5 | -2917.1 | 328.2 | -328.2 | 18584 | -0.29 | -0.50 | -0.50 | -0.50 | 0.17 | 202.2 | 1.00 | 1.00 |

subgroup. For these, the threshold densities are much higher and exceed the inferred maximum central density, suggesting that direct URCA processes of the type given by Eq. (26) would not be allowed in these cases (with the exception of SLy9 and SLy230a). However, we note that there are alternative direct URCA processes involving hyperons when the threshold density for these to appear has been passed (see Table IV and the related discussion). These provide an alternative rapid cooling mechanism.

IV. CONCLUSIONS

In this paper, we have examined the performance of 87 published parameter sets for the Skyrme interaction when used for calculating the general properties of infinite nuclear matter and of neutron stars. The parameter values are usually obtained by fitting to the ground-state properties of doubly closed-shell finite nuclei and of SNM at saturation. In order to improve the credibility of these density-dependent effective interactions when used for exotic nuclei (which are far from β stability, with proton-neutron ratios differing considerably from unity and with deviations expected from a uniform density distribution), it is desirable to extend the fitting data to include the density dependence of properties of asymmetric nuclear matter (of which neutron-star matter is an

example) since this represents the opposite extreme to that of doubly closed-shell nuclei. The Skyrme parameters are highly correlated and it is not possible to single out relationships between individual parameters and particular observed physical properties. However, it can be argued that if a certain set gives a good fit for both finite nuclei *and* asymmetric nuclear matter, then it has more chance of being successful for describing the properties of nuclei close to the neutron drip line.

Our analysis has shown that a key property for distinguishing among the Skyrme parametrizations is the density dependence of the symmetry energy, represented by the asymmetry parameter a_s in the present work. There are two fundamentally different trends: for group I, a_s is monotonically increasing with increasing density of the nuclear matter whereas for groups II and III it becomes decreasing at the higher densities. Furthermore, the rate of this decrease, which is dependent on the relative pattern of density dependences of the energy per particle in SNM and PNM, is an additional fingerprint distinguishing groups II and III. All of the other calculated properties are correlated with the behavior of a_s , including the chemical potentials, the particle composition of equilibrium dense matter, and the ability to produce viable neutron-star models.

No direct experimental evidence is yet available to determine which of these two trends is actually occurring in nature, although the situation may change rather soon [34]. However, taking into account that both the “realistic” potentials and the RMF model calculations consistently predict that a_s increases with increasing density and that interactions with this behavior give neutron star models in broad agreement with observations, we conclude that this is the more realistic scenario.

Out of the 87 Skyrme parametrizations which we have tested, only 27 give this behavior. We list these parameter sets in Table VII, together with the values of the incompressibility coefficient at saturation K_∞ and the isoscalar and isovector effective masses. This table demonstrates that it is not possible to set limits for “permitted” values of the individual Skyrme parameters within which they must lie in order for the interaction to be in line with the conditions discussed above. The reason is that the asymmetry coefficient a_s is a function of all of the nine parameters examined here,

$$\begin{aligned}
 a_s = & \frac{1}{3} \frac{\hbar^2}{2m} \left(\frac{3\pi^2}{2} \right)^{2/3} n^{2/3} - \frac{1}{8} t_0 (2x_0 + 1) n \\
 & - \frac{1}{24} \left(\frac{3\pi^2}{2} \right)^{2/3} [3t_1 x_1 - t_2 (5x_2 + 4)] n^{5/3} \\
 & - \frac{1}{48} t_3 (2x_3 + 1) n^{\alpha+1}.
 \end{aligned} \tag{27}$$

The parameters always act together as a correlated set, which is a characteristic feature of many-parameter effective interactions. We suggest that rather than developing new specialized parametrizations fitted to only a selection of experimental data (such as nuclear masses), it is more fruitful to

concentrate on those existing interactions which have been proven against the most general collection of experimental data for both finite nuclei and infinite nuclear matter. The present focus of low-energy nuclear physics is directed towards phenomena at the limits of the existence of bound nuclei, which are being investigated with radioactive beams. In this context, the approach of interest is that of mean-field theories which utilize density-dependent effective interactions, valid over a broad range of densities away from nuclear saturation density.

As far as comparison with the results of RMF theories and of the much more elaborate “realistic” potential approaches is concerned, we do not find any serious difference between them and the selected Skyrme models (group I) for prediction of the properties of nuclear matter and of neutron stars in the region of densities where the Skyrme approach is valid. This conclusion is rather worrying and poses an important question: Do the implementations of the theories at the region of densities, where the Skyrme approach used here is valid, all have so many adjustable parameters that the physics is obscured and no new insights are possible?

ACKNOWLEDGMENTS

This research was sponsored by the U.S. Department of Energy Grant No. DE-FG02-94ER40834; Division of Nuclear Physics, U.S. Department of Energy under Contract No. DE-AC05-00OR 22725 managed by UT-Battelle, LLC; the UK EPSRC; the Italian Ministero dell’Istruzione, dell’Università e della Ricerca and INFN; and the EU Program “Improving the Human Research Potential and the Socio-Economic Knowledge Base” (RTN Contract No. HPRN-CT-2000-00137).

-
- [1] H. Heiselberg and M. Hjorth-Jensen, *Phys. Rep.* **328**, 237 (2000).
 - [2] J.M. Lattimer and M. Prakash, *Phys. Rep.* **334**, 121 (2000).
 - [3] H. Heiselberg and V. Pandharipande, *Annu. Rev. Nucl. Part. Sci.* **50**, 481 (2000).
 - [4] V.G.J. Stoks, R.A.M. Klomp, C.P.F. Terheggen, and J.J. de Swart, *Phys. Rev. C* **49**, 2950 (1994).
 - [5] R.B. Wiringa, V.G.J. Stoks, and R. Schiavilla, *Phys. Rev. C* **51**, 38 (1995).
 - [6] R. Machleidt, F. Sammarruca, and Y. Song, *Phys. Rev. C* **53**, R1483 (1996).
 - [7] B.D. Day and R.B. Wiringa, *Phys. Rev. C* **32**, 1057 (1985).
 - [8] M. Baldo, G.F. Burgio, and H.-J. Schulze, *Phys. Rev. C* **61**, 055801 (2000).
 - [9] I. Vidana, A. Polls, A. Ramos, L. Engvik, and M. Hjorth-Jensen, *Phys. Rev. C* **62**, 035801 (2000).
 - [10] F. de Jong and H. Lenske, *Phys. Rev. C* **57**, 3099 (1998).
 - [11] V.R. Pandharipande and R.B. Wiringa, *Rev. Mod. Phys.* **51**, 821 (1979).
 - [12] R.B. Wiringa, V. Fiks, and A. Fabrocini, *Phys. Rev. C* **38**, 1010 (1988).
 - [13] A. Akmal and V.R. Pandharipande, *Phys. Rev. C* **56**, 2261 (1997).
 - [14] A. Akmal, V.R. Pandharipande, and D.G. Ravenhall, *Phys. Rev. C* **58**, 1804 (1998).
 - [15] V. R. Pandharipande and D. G. Ravenhall, in *Proceedings of a NATO Advanced Research Workshop on Nuclear Matter and Heavy Ion Collisions, Les Houches*, edited by M. Soyeur *et al.*, (Plenum, New York, 1989), p. 103.
 - [16] J.M. Lattimer, C.J. Pethick, D.G. Ravenhall, and D.Q. Lamb, *Nucl. Phys.* **A432**, 646 (1985).
 - [17] C.J. Pethick, D.G. Ravenhall, and C.P. Lorenz, *Nucl. Phys.* **A585**, 675 (1995).
 - [18] H. Krivine, J. Treiner, and O. Bohigas, *Nucl. Phys.* **A336**, 155 (1980).
 - [19] P. Bonche and D. Vautherin, *Nucl. Phys.* **A372**, 496 (1981); *Astron. Astrophys.* **112**, 268 (1982).
 - [20] N. K. Glendenning, *Compact Stars*, 2nd edition (Springer, New York, 2000).
 - [21] M. Onsi, H. Przysieznik, and J.M. Pearson, *Phys. Rev. C* **50**, 460 (1994); **55**, 3139 (1997).
 - [22] D. Vautherin and D.M. Brink, *Phys. Rev. C* **5**, 626 (1972).
 - [23] E. Chabanat, P. Bonche, P. Hansel, J. Meyer, and R. Schaeffer, *Nucl. Phys.* **A627**, 710 (1997).

- [24] J. Heyer, T.T.S. Kuo, J.P. Shen, and S.S. Wu, Phys. Lett. B **202**, 465 (1988).
- [25] M.F. Jiang, S.D. Yang, and T.T.S. Kuo, Phys. Lett. B **223**, 5 (1989).
- [26] J. Ventura, A. Polls, X. Vinas, S. Hernandez, and M. Pi, Nucl. Phys. A **545**, 247 (1992).
- [27] P.D. Stevenson, M.R. Strayer, and J. Rikovska Stone, Phys. Rev. C **63**, 054309 (2001).
- [28] J. Rikovska Stone, P.D. Stevenson, J.C. Miller, and M.R. Strayer, Phys. Rev. C **65**, 064312 (2002).
- [29] K. Sumiyoshi, D. Hirata, H. Toki, and H. Sagawa, Nucl. Phys. A **552**, 437 (1993).
- [30] T. Suzuki *et al.*, Phys. Rev. Lett. **75**, 3241 (1995).
- [31] T. Suzuki, H. Geissel, O. Bochkarev, L. Chulkov, M. Golovkov, N. Fukunishi, D. Hirata, H. Irnich, Z. Janas, H. Keller, T. Kobayashi, G. Kraus, G. Munzenberg, S. Neumaier, F. Nickel, A. Ozawa, A. Piechaczek, E. Roeckl, W. Schwab, K. Summerer, K. Yoshida, and I. Tanihata, Nucl. Phys. A **630**, 402c (1998).
- [32] B.A. Brown, Phys. Rev. Lett. **85**, 5296 (2000).
- [33] Bao-An Li, C.M. Ko, and Z. Ren, Phys. Rev. Lett. **78**, 1644 (1997).
- [34] Bao-An Li, Phys. Rev. Lett. **88**, 192701 (2002).
- [35] P. G. Reinhard (unpublished).
- [36] C.M. Ko, H.C. Pauli, M. Brack, and C.E. Brown, Nucl. Phys. A **236**, 269 (1974).
- [37] M. Beiner, H. Flocard, N. Van Giai, and P. Quentin, Nucl. Phys. A **238**, 29 (1975).
- [38] M.J. Giannoni and P. Quentin, Phys. Rev. C **21**, 2076 (1980).
- [39] Nguyen Van Giai and H. Sagawa, Phys. Lett. **106B**, 379 (1981).
- [40] J. Bartel, P. Quentin, M. Brack, C. Guet, and H.-B. Hakansson, Nucl. Phys. A **386**, 79 (1982).
- [41] M. Rayet, M. Arnould, F. Tondeur, and G. Paulus, Astron. Astrophys. **116**, 183 (1982).
- [42] F. Tondeur, M. Brack, M. Farine, and J.M. Pearson, Nucl. Phys. A **420**, 297 (1984).
- [43] J. Dobaczewski, H. Flocard, and J. Treiner, Nucl. Phys. A **422**, 103 (1984).
- [44] J. Friedrich and P.-G. Reinhard, Phys. Rev. C **33**, 335 (1986).
- [45] L. Bennour, P.-H. Heenen, P. Bonche, J. Dobaczewski, and H. Flocard, Phys. Rev. C **40**, 2834 (1989).
- [46] J.M. Pearson, Y. Aboussir, A.K. Dutta, R.C. Nayak, and M. Farine, Nucl. Phys. A **528**, 1 (1991).
- [47] Y. Aboussir, J.M. Pearson, A.K. Dutta, and F. Tondeur, Nucl. Phys. A **549**, 155 (1992).
- [48] P.-G. Reinhard and H. Flocard, Nucl. Phys. A **584**, 467 (1995).
- [49] E. Chabanat, Ph. D. thesis, Lyon, 1995.
- [50] J.M.G. Gomez and M. Casas, Few-Body Syst., Suppl. **8**, 374 (1995).
- [51] W. Nazarewicz, J. Dobaczewski, T.R. Werner, J.A. Maruhn, P.-G. Reinhard, K. Rutz, C.R. Chinn, A.S. Umar, and M.R. Strayer, Phys. Rev. C **53**, 740 (1996).
- [52] B.A. Brown, Phys. Rev. C **58**, 220 (1998).
- [53] P.-G. Reinhard, D.J. Dean, W. Nazarewicz, J. Dobaczewski, J.A. Maruhnand, and M.R. Strayer, Phys. Rev. C **60**, 014316 (1999).
- [54] F. Tondeur, S. Goriely, J.M. Pearson, and M. Onsi, Phys. Rev. C **62**, 024308 (2000).
- [55] M. Rashdan, Mod. Phys. Lett. A **15**, 1287 (2000).
- [56] S. Goriely, F. Tondeur, and J.M. Pearson, At. Data Nucl. Data Tables **77**, 311 (2001).
- [57] J.M. Pearson and S. Goriely, Phys. Rev. C **64**, 027301 (2001).
- [58] M. Samyn, S. Goriely, P.-H. Heenen, J.M. Pearson, and F. Tondeur, Nucl. Phys. A **700**, 142 (2002).
- [59] J. Margueron, J. Navarro, and Nguyen Van Giai, Phys. Rev. C **66**, 014303 (2002).
- [60] M. Farine, J.M. Pearson, and F. Tondeur, Nucl. Phys. A **696**, 396 (2001).
- [61] G. Baym, C. Pethick, and P. Sutherland, Astrophys. J. **170**, 299 (1971).
- [62] W.D. Arnett and R.L. Bowers, Astrophys. J., Suppl. Ser. **33**, 415 (1977).
- [63] V.R. Pandharipande, Nucl. Phys. A **178**, 123 (1971).
- [64] S. Balberg, I. Lichtenstadt, and G.B. Cook, Astrophys. J., Suppl. Ser. **121**, 515 (1999).
- [65] R.B. Wiringa, Rev. Mod. Phys. **65**, 231 (1993).
- [66] C.M. Keil, F. Hoffmann, and H. Lenske, Phys. Rev. C **61**, 064309 (2000).
- [67] M. Hanauske, D. Zschesche, S. Pal, S. Schramm, H. Stocker, and W. Greiner, Astrophys. J. **537**, 958 (2000).
- [68] R.C. Tolman, Proc. Natl. Acad. Sci. U.S.A. **20**, 3 (1934); J.R. Oppenheimer and G.M. Volkov, Phys. Rev. **55**, 374 (1939).
- [69] R. Schaffer, Y. Declais, and S. Julian, Nature (London) **300**, 142 (1987).
- [70] P. Haensel and J.L. Zdunik, Nature (London) **340**, 617 (1989).
- [71] P. Haensel, M. Salgado, and S. Bonazzola, Astron. Astrophys. **296**, 745 (1995).
- [72] R. Koncewicz, Project report (unpublished).
- [73] C.J. Pethick, Rev. Mod. Phys. **64**, 1133 (1992).
- [74] J.M. Lattimer and M. Prakash, Astrophys. J. **550**, 426 (2001).
- [75] M. Prakash *et al.*, Phys. Rep. **280**, 1 (1997).
- [76] F. Mandl, *Statistical Physics*, 2nd ed. (Wiley, New York, 1988), p. 285.
- [77] F. Weber, *Pulsars as Astrophysical Laboratories for Nuclear and Particle Physics* (IOP, Bristol, 1999), Chap. 7, 63.
- [78] G. Bao, L. Engvik, M. Hjorth-Jensen, E. Osnes, and E. Ostgaard, Nucl. Phys. A **575**, 707 (1994).
- [79] V. Canuto, Annu. Rev. Astron. Astrophys. **13**, 335 (1995).
- [80] N.K. Glendenning, Astrophys. J. **293**, 470 (1985).
- [81] T.M. Braje and R.W. Romani, Astrophys. J. **580**, 1043 (2002).
- [82] J.A. Faber, P. Grandclement, F.A. Rasio, and K. Taniguchi, Phys. Rev. Lett. **89**, 231102 (2002).
- [83] M. Prakash, M. Prakash, J.M. Lattimer, and C.J. Pethick, Astrophys. J. Lett. **390**, L77 (1992).
- [84] M. Prakash, Phys. Rep. **242**, 191 (1994).
- [85] P.B. Jones, Phys. Rev. D **64**, 084003 (2001).